



ELECTROENCEPHALOGRAPHY:
SUBDURAL MULTI-ELECTRODE BRAIN CHIP

Thesis

John E. Rosenstengel
Captain, USAF

AFIT/GE/ENG/95D-22

DISTRIBUTION STATEMENT A

Approved for public release
Distribution Unlimited

DEPARTMENT OF THE AIR FORCE
AIR UNIVERSITY
AIR FORCE INSTITUTE OF TECHNOLOGY

Wright-Patterson Air Force Base, Ohio

DTIC QUALITY INSPECTED 1

AFIT/GE/ENG/95D-22

ELECTROENCEPHALOGRAPHY:
SUBDURAL MULTI-ELECTRODE BRAIN CHIP

Thesis

John E. Rosenstengel
Captain, USAF

AFIT/GE/ENG/95D-22

19960426 062

The views expressed in this thesis are those of the author and do not reflect the official
policy or position of the Department of Defense or the U.S.

AFIT/GE/ENG/95D-22

ELECTROENCEPHALOGRAPHY:
SUBDURAL MULTI-ELECTRODE BRAIN CHIP

THESIS

Presented to the Faculty of the Graduate School of Engineering
of the Air Force Institute of Technology
Air University
In Partial Fulfillment of the
Requirements for the Degree of
Master of Science in Electrical Engineering

John E. Rosenstengel, B.S.E.E.
Captain, USAF

December, 1995

Approved for public release; distribution unlimited

Contents

1	Introduction	1
1.1	Justification	1
1.2	Problem Statement and Scope	3
1.3	Order of Presentation	3
2	Human Brain	4
2.1	Physiology of Selected Structures	4
2.1.1	Cerebellum	5
2.1.2	Thalamus	5
2.1.3	Hypothalamus	6
2.1.4	Amygdala and Hippocampus	6
2.1.5	Cerebral Cortex	7
2.2	Time Perception	8
2.3	Memory Processes	10
2.4	Conclusions	10
3	Brain Chip	12
3.1	History	12
3.2	Related Work	12
3.3	Reference Chip	13
3.3.1	Design	13
3.3.2	Testing	16
3.4	Differential Chip	19
3.4.1	Design	19

3.4.2	Testing	22
3.5	Passivation	23
3.5.1	Electrode Protection	23
3.5.2	Encapsulation	24
3.6	Final Packaging	24
3.7	Conclusions and Recommendations	25
4	Methodology	26
4.1	Introduction	26
4.2	Implantation and Testing	26
4.2.1	Test Instrumentation	26
4.3	Development of Test Scenarios	27
4.3.1	Averaged Evoked Response (AER) Test	27
4.3.2	Apparent Motion Test Setup	28
4.4	Data Collection	29
4.5	Conclusions	30
5	Results and Conclusions	31
5.1	Surgery	31
5.2	Results	32
5.2.1	Averaged Evoked Response	32
5.2.2	Phase Reversal	34
5.2.3	Post Noise Saturation Period	36
5.3	Conclusion	38
A	C-Code for Test Scenario Control	39
B	Protocol	48
C	Post-processing steps	58
C.1	Standard Clean	58
C.2	Metalization Process	58
C.3	Polyimide Application Process	59

C.4 Packaging	60
D Training Pulse Coupled Neural Networks	62
D.0.1 Basic Design	62
D.0.2 Learning Laws	64

List of Figures

1.1	Handwritten Numeral '0'	2
2.1	Human Brain	4
2.2	Subjective Referral in Time	9
3.1	Photograph of Referenced Brain Chip	14
3.2	Stylized Representation of Reference Chip Design	15
3.3	Microprobe Placement	17
3.4	Circuit of Source Impedance Measurement	17
3.5	Photograph of Differential Brain Chip	19
3.6	Stylized Version of the Differential Chip Design	21
3.7	Oscilloscope Traces of Output Signal from Differential Chip	22
3.8	Oscilloscope Traces of Noisy Output Signal from Differential Chip	23
4.1	Test Equipment Set Up	26
4.2	Averaged Evoked Response	28
4.3	Over-sampling the Multiplexed Output	29
5.1	Labeled Baboon Brain	31
5.2	Clock Noise Measured with Brain Chip	32
5.3	Single Sensor Measurement	33
5.4	Recorded Averaged Evoked Response, First Chip	33
5.5	Recorded Averaged Evoked Response	34
5.6	Recorded Averaged Evoked Response (Top vs. Bottom)	35
5.7	Recorded Averaged Evoked Response (Right vs. Left)	35

5.8 Recorded Averaged Evoked Response (Every Other)	36
5.9 Every Other Sensor Selection	37
5.10 Recorded Signals After Noise Saturation	37
D.1 Pulse Coupled Neural Network	63

List of Tables

2.1	Purported Functions of the Hypothalamus	6
2.2	Hemispheric Specializations of Human Cerebral Cortex	7
3.1	Requirements for Reference Chip	13
3.2	Requirements for Differential Chip	20
C.1	Cure times for final application of polyimide.	61

Abstract

In October 1995, a CMOS brain chip consisting of two 8×17 multiplexed sub-arrays designed to measure electrical potentials at the cortical column level, was implanted on the somatosensory cortex of a laboratory rhesus monkey. Electroencephalograph (EEG) and averaged evoked response (AEG) data were taken over a period of 40 minutes. The brain chip was replaced with an identical chip, and data were again taken for 40 minutes. In both instances AEG signals of approximately $150 \mu V_{pp}$ were recorded. Additionally, the first implanted chip recorded three phases of data: 1) AEG; 2) large clock noise (during a period where the chip appears to have burned the cortex); 3) AEG-like signals of magnitude, $\approx 100 \mu V_{pp}$, with substantially improved signal to noise ratio.

All data were taken while the monkey was under general anesthesia. The monkey was euthanized immediately after the experiments, due to a pre-existing abdominal cancer.

ELECTROENCEPHALOGRAPHY: SUBDURAL MULTI-ELECTRODE BRAIN CHIP

1. Introduction

1.1 Justification

The creation of highly autonomous and reliable computer systems for weapons control and information processing may require new knowledge of the human brain. Man has created digital engines capable of performing highly repetitive and, in some cases, extremely complex tasks in a fraction of the time required for a human. Yet, the fundamental limitation of these machines is that all possible variation must be predicted by the programmer, so that the computing system has instructions for handling all situations. The challenge is to build a system wherein the programmer does not have to foresee all outcomes, and the computer can handle novel situations.

The field of pattern recognition, determining the presence of a particular signal based on patterns in information, has many of these same challenges and would benefit greatly from advances in 'intelligent' processing. An example, pertinent to the intelligence community is text reading. Considering an automated text reader with an accuracy rate of 99% (reasonable for a given set of text with a specific amount of distortion—such as facsimile distortion), and the fact that each page of a document can easily contain more than 1,000 characters, we would expect at least 10 character recognition errors per page. By way of comparison, a human will typically avoid all character errors. Accuracy, therefore, dictates that a human proof read the results. This being the case, it is often advantageous to simply use humans to type in the data without machine assistance.

This limitation is seen in the seemingly simple task of reading handwritten zip codes. Figure 1.1 shows a digitized image of a poorly written numeral '0' that is consistently mistaken as a numeral '2' by many pattern recognition systems considered to have reasonable performance. However, it does not *look* like a '2,' implying that humans use different features to recognize numerals than the machines in question. It should be obvious that this

error could be corrected by using different features, possibly Fourier coefficients, instead of those used in the example systems. However, changing the features, or even simply adding new features, typically causes different errors. Given the problems exhibited by man-made machines, we must ask, “How can people *know* that Figure 1.1 is a ‘0’?”

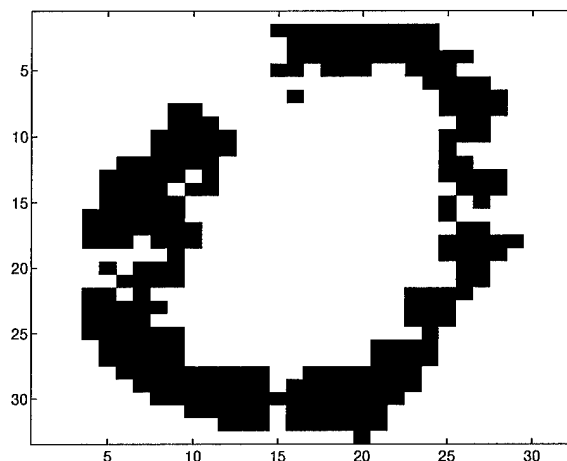


Figure 1.1: Handwritten numeral ‘0’ that is mistaken for a numeral ‘2’ by pattern recognition systems

Whether due to its chosen feature space, preprocessing algorithms, classification algorithm, or vastly parallel structure, the human brain is the premiere pattern recognition machine. Humans can recognize familiar patterns in a wide range of situations, including time distortions, position changes, rotation and scale variances, and others.

Beyond simple pattern recognition, a human’s ability to take novel input and create associations based on that input in order to keep a running model of its environment, makes it the most powerful decision making device known.

Information about how the brain takes raw sensory information and processes it, may translate to great advances for:

- Intelligence–image analysis, character reading, and message detection
- Weapons development–autonomous cruise missiles, and local detection of enemy forces
- Health–cancer detection, and other laboratory tests
- Military maneuvers–weather forecasting, battle simulation, and chemical/biological agent detection.

1.2 Problem Statement and Scope

The Air Force must be able to record how the human brain works at the proper level of processing to begin to model the genius that lies within.

The efforts supporting this thesis are directed at the ultimate goal of improving existing pattern recognition systems, by gaining new knowledge of the brain's activity. Toward this goal, AFIT is working to organize current biological information and existing neural network simulation algorithms into successively more accurate models of human mental function. By utilizing past brain chip work (see chapter 3, page 12) to bring AFIT's information gathering capabilities directly to the cortical surface, this thesis represents a significant contribution.

The specific goals of this thesis are:

1. Test and verify the performance of newly developed brain chips prior to preparation for implantation.
 - Voltage gain from the sensor pads to the output.
 - Leakage noise from one sensor pad to its neighbors.
 - Operational range of voltage measurement.
2. Successfully implant the brain chip onto the sensory cortex of a test animal.
 - Passivation—to prevent damaging interactions between brain and brain chip.
 - Packaging of the implantable device.
 - Implantation.
3. Verify the performance and utility of the brain chip by taking averaged evoked response data
4. Run apparent motion experiments on the test subject and analyze the recorded results

1.3 Order of Presentation

Chapter 2, page 4, provides a brief review of the physiology of the brain. Chapter 3, page 12, describes the development, design and preparation of the AFIT multi-electrode brain chip. Chapter 4, page 26, describes the preparation for implantation and tests run on the implanted test animal. Chapter 5, page 31, discusses the results and makes recommendations for future efforts.

2. Human Brain: Basic Form and Function

The human brain is not a monolithic black-box for information processing. It has definite substructure and specialized functionality, indicated by a wealth of research and the hands-on experiences of brain surgery. Figure 2.1 shows a detailed breakdown of brain components. This section will describe a number of these components and provide a description of the functions attributed to each.

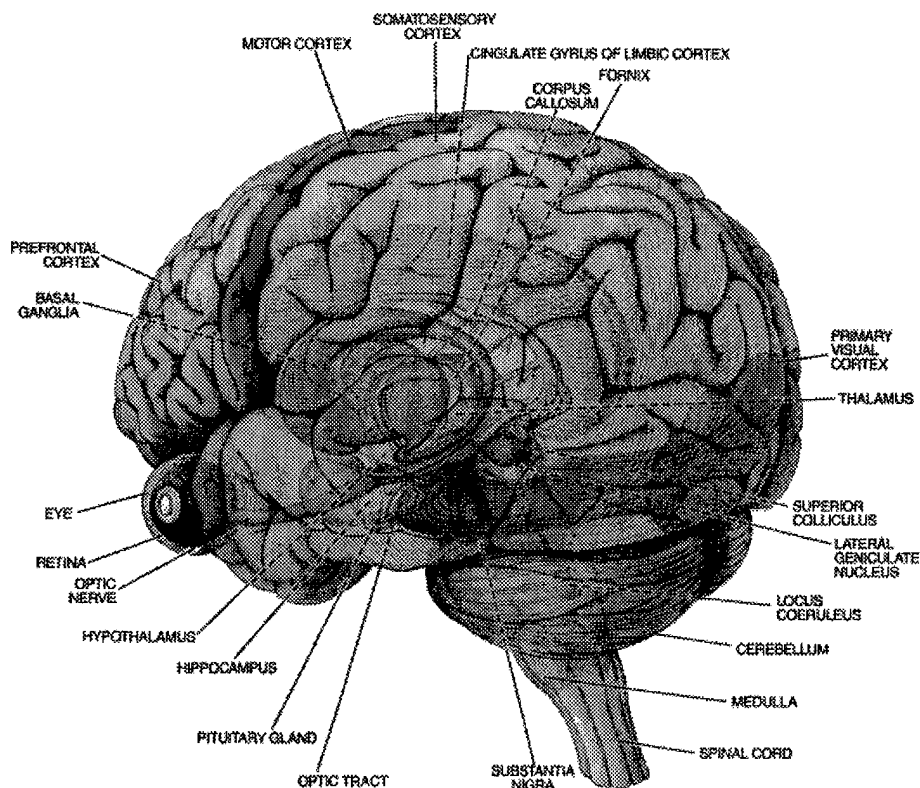


Figure 2.1: Human Brain [13]

2.1 Physiology of Selected Structures

There are many divisions and subdivisions within the human brain. A complete discussion is beyond the scope of this thesis. The reader is encouraged to read more [8]. Therefore, this section is restricted to the cerebellum, thalamus, hypothalamus, amygdala, hippocampus, and cerebral cortex.

2.1.1 Cerebellum.

The cerebellum sits at the back of the brain as an appendage of the rhombencephalon, or hindbrain. According to Kapit [8], the cerebellum is the major structure for motor coordination. It acts as a big comparator, checking the activity of all voluntary muscles against the commands sent to them and offering suggested corrections. The cerebellum's position between the forebrain and the spinal cord allows it to perform its tasks rapidly, providing grace and precision of movement.

2.1.2 Thalamus.

The thalamus is the crossroads of the brain. Centrally located, it has connections to most, if not all, areas of the cortex [15, 17]. The thalamus has a number of subdivisions that correspond to different structures, mainly subdivisions of the cerebral cortex [15].

The case of Karen Ann Quinlan, who had the misfortune of being in a persistent vegetative state for 10 years, has given new insight into the role of the thalamus. Dr. Kinney and associates report that, though Ms. Quinlan experienced waking and sleeping states, marked by increased eye movement and brain activity, she never achieved consciousness [9]. Autopsy findings revealed relatively little damage in the cortex but profound damage in the sub-cortical thalamus [9]. Thus, the conclusion that the thalamus appears to play a substantial role in consciousness follows.

Dr. Ojemann has found that the thalamus has connections to most, if not all cortical areas, particularly those involved in language skills [18]. In most studies he was able to elicit the same language impairments by electrically stimulating the thalamus, as he could by stimulating the cortex. Furthermore, some experiments indicate that the thalamus was also acting to focus attention on particular information [18].

Again, most, if not all, portions of cerebral cortex have connections *from* as well as *to* the thalamus [12, 15, 16]. These connections establish what is called thalamo-cortical loops. These loops are the mechanism for information processing (where areas of cortex keep their current hypothesis of what's happening), memory storage, and possibly the advent of consciousness itself [12, 15, 16].

Dr. Mumford explains the basic architecture for thalamus functions, particularly in reference to the thalamo-cortical loops [15, 16].

- Cortical areas learn recurring patterns.

- Cortical areas continually try to analyze the present situation in terms of these patterns, generating hypotheses that often conflict.
- These hypotheses are sent to the thalamus where a kind of voting takes place.
- The consensus is broadcast back to the cortex as an updated view of that aspect of the world dealt with by that area of cortex [16].

2.1.3 Hypothalamus.

The hypothalamus is a protrusion of the thalamus and has been referred to as “the head ganglion of the sympathetic nervous system” by Dr. Charles Sherrington [8]. Table 2.1 describes the functions attributed to the hypothalamus.

Table 2.1: Purported Functions of the Hypothalamus [8]

Function	Description and Source
Sympathetic Responses	Areas control fight or flight response. Investigated by electrical stimulation.
Sexual Behavior	Stimulating or destroying sections effects regulation of sex hormones.
Diurnal Rhythms	Areas respond to light stimuli and help with sleeping and waking.
Feeding Behavior	Stimulation causes increased appetite.
Drinking Behavior	Stimulation or acetylcholine injection induces drinking. Destruction causes problems with water retention and imbalances in electrolytes.
Body Temperature Regulation	This appears to be the center of body temperature regulation.
Hormonal Regulation	Parts act like an endocrine gland.

2.1.4 Amygdala and Hippocampus.

Located beneath the olfactory cortex, the amygdala and hippocampus extend into both hemispheres of the brain. Patient experience following brain surgery indicates that these structures are crucial to memory formation [14].

Following surgery to control epileptic seizures, every human patient with post-operative retrograde amnesia (the inability to form new memories) had suffered incidental damage to the hippocampus during the surgical procedure [14].

Animal studies, performed by Dr. Mishkin, Chief of the Laboratory of Neuropsychology at the National Institute of Mental Health, have provided further insight into the functions of the amygdala and hippocampus [14]. In preliminary studies it was found that the removal of

only one of the structures, be it the amygdala or hippocampus, had little effect on memory processes. “Animals whose amygdala alone had been removed were slow to learn the association of stimulus and reward, but they were still able to do so” [14]. In order to dramatically increase impairment and produce full retrograde amnesia in a macaque monkey, both structures had to be damaged [14]. In contrast, just damaging a human hippocampus alone can produce full retrograde amnesia [14].

2.1.5 Cerebral Cortex.

Unique to mammals, the cerebral cortex is usually viewed as the home of higher thought processes. The human cortex is the place where higher thought processes occur: sensory information is broken apart and analyzed, problems are solved, and language is processed.

Table 2.2 shows the highest division and specialization of the cortex, the left vs. right hemisphere. Dr. Kaput reports that 97 percent of all humans have a dominant left hemisphere for speech [8].

Table 2.2: Hemispheric Specializations of Human Cerebral Cortex [8]

Left	Right
Verbal	Representational
Motor Dominant	Emotional
Logical	Humorous
Analytical	Holistic
Linear	Visual/Spatial
Temporal	Musical

Though there are many other detailed processes of the cortex the discussion will focus on functions related to this thesis.

The cortex has subdivisions particular to specific functions: somatosensory, language, vision, auditory processing, etc. Each of these is further subdivided into specialized functional areas that are connected to each other in a reciprocal manner (if A goes to B then B goes to A) [16]. Dr. Mumford divides the connections into three types of pathways.

- Ascending pathways: going from a higher area (level that is more abstracted from the sensory data or immediate motor commands) to a lower area (level that is more directly connected and related to sensory data or immediate motor commands).
- Descending pathways: going from lower to higher areas.
- Additional descending: going from higher areas to lower areas where the difference in abstraction is not readily apparent [16].

The ascending pathways allow detailed information about stimuli to be abstracted into more general concepts and into the 'language' of the higher area. Dr. Mumford hypothesizes the descending pathways translate their hypothesis of what is happening back to the lower area, in its language, as a template to allow comparison, so that hypotheses may be competed. He also hypothesizes that the additional descending pathways might carry residual, or unexplained portions of the sensory data, to allow a more global (outside the sending area's scope) hypothesis to be generated [16]. This would be analogous to asking an equal what their opinion is for something you cannot explain.

The cortico-cortical loops can be modeled based on Dr. Mumford's architecture, using standard artificial neural networks for connections in a looping fashion. The higher area can create an image of the lower level's data by making a conglomeration of templates (like placing templates of trees on top of a template of a deer) and handing it back to the lower level for comparison. The lower level will compare and excite the higher level in areas that are missing in the conglomeration, and inhibit areas that are extraneous (existing in the conglomeration, but not in the sensory information). This looping action will allow convergence on a solution to the question, "What am I looking at?"

The basic computing elements in the cortex are the cortical columns [7]. These columnar groups of neurons were reported by Vernon B. Mountcastle, in the somatosensory cortex, and by David H. Hubel and Torsten N. Wiesel, in the visual cortex [5]. Estimates of the size vary in species, as well as cortical section, in the range $50\text{ }\mu\text{m}$ to $500\text{ }\mu\text{m}$ [20].

2.2 Time Perception

Perception is psychosomatic. That is, perception is all in your head. Visual, auditory, tactile, and taste perception are just a few of the illusions that humans make for themselves, to allow them to interpret the sensory input that they are bombarded with. Along the same lines, time is a confabulation of the brain that allows us to bind sensory information from one instance to another. While this may seem a presumptuous statement, the work of Dr. Benjamin Libet lends substantial credence [10, 11].

Figure 2.2 shows the results of Dr. Libet's experiments concerning subjective referral of time [11]. Dr. Libet reports that, while a delay of approximately 500 milliseconds occurs before conscious perception of the stimuli, the conscious experience of the stimuli is subjectively

referred back in time to approximately the actual stimulus [10, 11]. The AER signal is the cortical response to a stimulus, discussed in section 4.3, page 27.

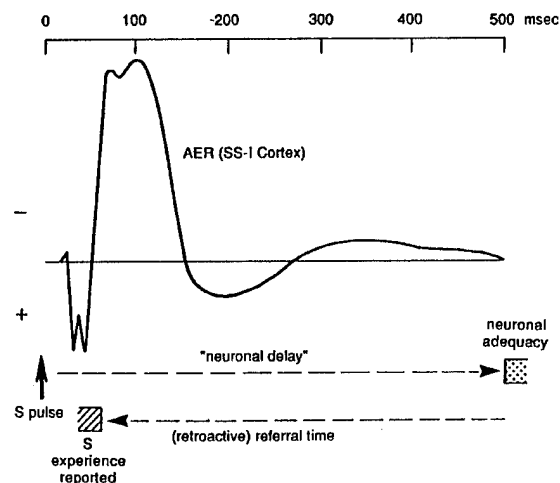


Figure 2.2: Subjective Referral in Time of a Conscious Event [10]

Dr. Libet's experimental results open a 1/2 second window in which external influences have an opportunity to affect the perception of a previous stimulus [11]. A profound example of external influences affecting perception is Geldard and Sherrick's cutaneous rabbit illusion [4]. In this illusion, a number of taps (approximately 5) are delivered at regular intervals to the wrist followed by additional taps further up the arm without breaking rhythm (40-60 msec between pulses) [4]. The subject perceives a series of evenly spaced taps reminiscent of a rabbit hopping from the location of the first taps to the location of the final taps [4]. While it is interesting that the first series of taps seems to affect the perceived location of later series' taps (suggesting that perception uses prior information to shape current perception), the critical indication is that subsequent series' taps appear to affect the perceived location of previous taps. This, in turn, suggests that the later taps occurred prior to the perception of the previous taps, giving the appearance of non-causal processing. In other words, the second series of taps causes taps from the first series to be perceived as moving in the direction of the second series' location. If perception were immediate, or even faster than 10's of milliseconds, then the brain would not know which direction to 'move' the first series' taps.

2.3 Memory Processes

Memory appears to have different forms including, but not limited to: immediate, short-term, long-term, and recognition memory [14]. As there is a vast quantity of information in current circulation about memory it is important to describe only those forms that are relative to this thesis. The thesis is concerned with immediate and short-term memory, because they seem to be required for perception of motion.

At the lowest-level, immediate memory of what you are sensing as the world changes, seems to be a function of habituation.

Among biological mechanisms that can encode temporal information, is a particularly simple and well-understood phenomenon known as habituation. Primarily, habituation is a means by which biological neural systems vary their synaptic strengths in order to ignore repetitive, irrelevant stimuli. Habituation serves as a novelty filter. [21]

While section 2.1, page 6, discussed the connection between the amygdala, hippocampus, and the ability to store new long-term memories, the storage location is central to the AFIT view of memory. The model views memory as the processing of information, and therefore, memory is expected to be stored in the processing areas of the cortex. Doctors Mishkin and Appenzeller report that the most likely location for memories is the cortical areas where sensory impressions take shape [14].

The sub-cortical memory circuits must therefore engage in a kind of feedback with the cortex. After a processed sensory stimulus activates the amygdala and hippocampus, the memory circuits must play back on the sensory area. That feedback presumably strengthens and so perhaps stores the neural representation of the sensory event that has just taken place. [14]

2.4 Conclusions

Mankind has acquired a great deal of knowledge regarding the brain's basic structure and function. Correlations are made between the actions of certain areas of the brain, and their observable effects. There is evidence of brain function found in large scale, due to damaged brain structure and large area electrical recording. The damage and recordings are compared with observable behavioral changes, like the ability to lay down the new memories required to learn new tasks, or the ability to recall old memories and use them to recognize family

members. This thesis effort seeks to leverage on this knowledge and advance the use of the AFIT multi-electrode brain chip to help discover some of the remaining unknowns:

- What is the form data takes on in the brain?
- Exactly how is data processed?
- How/where is data stored and retrieved?

3. Brain Chip Development and Testing

AFIT's brain chip is a tool for direct measurement of electroencephalogram (EEG) data at the cortical surface. It was designed to allow observers to view, electrically, the cerebral cortex at approximately the cortical column scale [7]. The brain chip presently allows for 256 spatially separated measurements in an area of less than a dime.

The actions recorded in this section achieve thesis goal number 1, page 3.

3.1 History

The brain chip effort began with a 4 x 4 array of electrodes that was placed directly on the visual cortex of a laboratory beagle (*Canis familiaris*) in 1982 [7]. The successful retrieval of electroencephalogram (EEG) and visually evoked response (VER) data energized the development of improved brain chips.

James Reid's 1993 thesis details the early history of the AFIT brain chip from Joseph Tattman's 1979 16-electrode design, that was not successfully fabricated, through Gary Fitzgerald's redesign and successful fabrication, to George German's effort to passivate the chip [19]. This work allowed Russell Hensley and David Denton, under the tutelage of Dr. Kabriski, to implant a chip in 'Ricky', a laboratory beagle [19]. Reid goes on to document improvements in design, including his work on the 16 x 16 array chip, referred to herein as the reference chip [19].

There are currently two designs that have been implemented and tested: the reference chip and the differential chip. The chips were fabricated through the Metal Oxide Semiconductor Implementation Service (MOSIS) using the 2.0 μm -wall process. Twenty four die of each design were returned with 4 die packaged in 40-pin dual in-line packages (DIPs).

3.2 Related Work

Much work has been done on cortical systems, however, the AFIT brain chip focuses on recording two dimensional cortical electroencephalographic data at the scale of the cortical column.

In 1966, DeMott reported his work on a toposcopic technique for studying the electrical activity of the cortex [1]. DeMott bundled 400 wires into an array with 1.5 millimeter on-center spacing, and placed them directly on the cortex of monkeys and cats, among others [1].

DeMott successfully recorded steep voltage gradients (up to 1 mV/mm) [1]. To make his measurements as precise as possible, DeMott used 400 individual differential (to eliminate any common-mode noise) amplifiers giving him a usable range of input signals from 50 to $500\text{ }\mu\text{V}_{pp}$ [1]. DeMott's measurements were taken from the visual cortex, to record visual evoked responses. The peak to peak voltages were typically in the range $200\text{--}500\text{ }\mu\text{V}_{pp}$, and showed repeated patterns in response to identical stimuli [1, 20].

Dr. Walter Freeman has collected EEG data from the olfactory cortex of rabbits using approximately 90 electrodes, spaced $500\text{ }\mu\text{m}$ apart [3]. Dr. Freeman recorded signals which could be correlated with 'recognized' scents that exhibited bursts of high frequency ($20\text{--}90\text{ Hz}$) activity with an amplitude of approximately $100\text{ }\mu\text{V}_{pp}$ [3].

3.3 Reference Chip

The reference chip, seen in figure 3.1, is so named because it takes one-sided measurements relative to the electrical potential of an L-shaped electrode.

3.3.1 Design.

The goals to be met by the reference chip are shown in Table 3.1 [19]. To meet the requirements concerning a limited number of input and output lines, the array is scanned, and output is multiplexed onto a single line.

Table 3.1: Requirements for Reference Chip [19]

Requirement	Reason	Implemented
Small size	Approximately match the size of individual cortical columns	dime sized
Bidirectional current flow	Allow both stimulation and recording of the cortex	Yes
Small number of I/O connections	Difficulty in making connections from inside the cranium to external circuitry	7
Number of I/O connections not dependent on the number of electrodes	Allows the number of electrodes to be increased without increasing the number of connections	Multiplexing
Capability to individually address the electrodes	Allows stimulation and recording to individual locations of the cortex	Yes

The reference chip (figure 3.2) consists of 256 electrodes arranged in a 16×16 array, two 4 to 16 decoders, sixteen transmission gates, an 8-bit counter, and an L-shaped reference

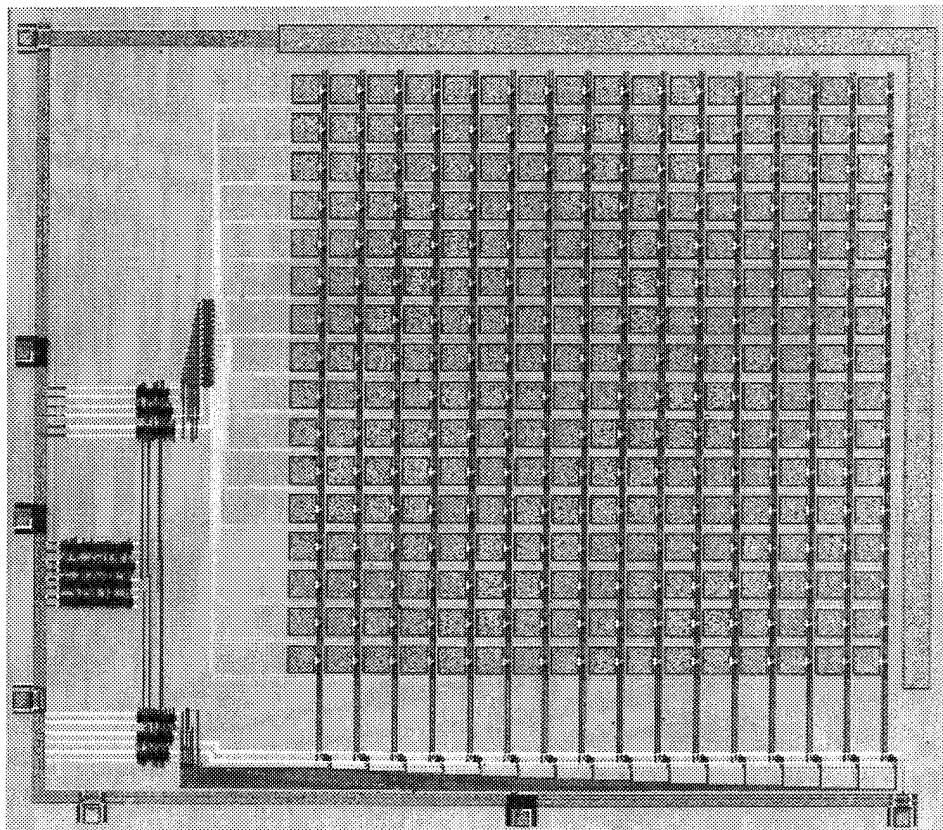


Figure 3.1: Photograph of Reference Chip

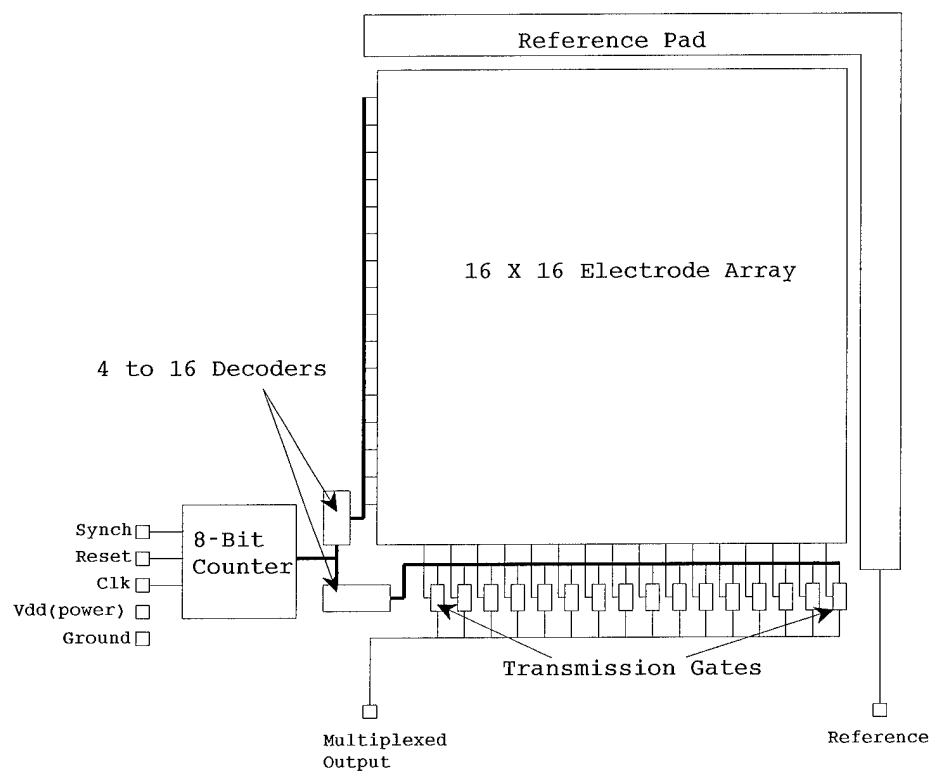


Figure 3.2: Stylized Representation of Reference Chip Design [20]

pad [19]. One 4 to 16 decoder uses the least significant bits of the 8-bit counter to select one of the 16 transmission gates to drive the multiplexed output line, scanning each column. The second 4 to 16 decoder is connected to the most significant bits of the 8-bit counter, selecting a row to be scanned [19]. The electrodes are spaced evenly at $250\ \mu m$ on center, which is the average of estimates for cortical column size given in chapter 2.1, page 8.

A substantial portion of the design and implementation work is discussed in the passivation section, section 3.5, page 23.

3.3.2 Testing.

Each lot of chips (reference and differential) received from the manufacturer was tested for validity of design, accurate implementation of the design and proper function prior to entering the time consuming encapsulation process (refer to section 3.5, page 23). Additionally, this testing includes discovery of properties of the implemented design that are required to adequately assess any results from tests conducted after implantation. These properties are the source impedance (amount of impedance between the sensor pad currently connected via the multiplexor to the output line and the multiplexor output line) and the leakage noise (the effect that the leakage current from a voltage potential on one sensor pad has on neighboring pads).

Verification of design and proper function was performed by placing a marker voltage, per figure 3.3, and taking measurements of the multiplexed output line. The marker voltage allowed the oscilloscope to be triggered consistently in sync with scanning. Proper operation of the counters was verified by changing the time base on the oscilloscope to allow an observer to count the number of clocks between marker signals (256 clocks/marker). To make certain that every row and column is scanned, the marker was placed on each pad of the main diagonal and output was verified with the oscilloscope. The output row sync performance was validated with the oscilloscope in much the same manner as counting. The row sync output was seen every 16 clock cycles.

Figure 3.3 shows where sources were placed and data were acquired directly to and from the chip's sensor pads, using a microprobe station. 'Marker' shows where a $5\ V_{dc}$ source was placed, on the first row and column to allow the oscilloscope to be triggered at a known time. V_{test} is where an alternating current source was placed to test the ability of the referenced brain chip to sample low voltage alternating current signals, like those expected on the cortical

surface. And, V_{noise} is where a probe was placed to measure leakage from the neighboring pad.

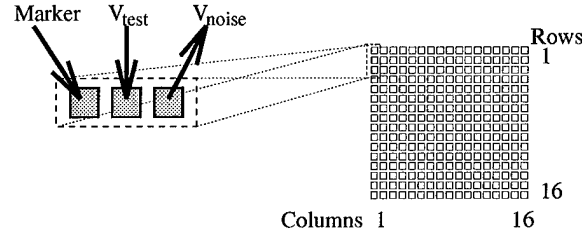


Figure 3.3: Microprobe placement for analog testing of the referenced brain chip

The source impedance causes a voltage difference between the sensor pad and the output line, because of voltage division between the source impedance and the impedance between the output signal and ground. Figure 3.4 shows the circuit for this test, as well as the method for producing the marker peak for all other tests. Using Ohm's Law, equation 3.1, a value for the combined impedance of the first and second (row and column) transistors, responsible for selecting each pad, can be calculated as approximately $33\text{ k}\Omega$. Further accuracy can be achieved by careful measurement of the voltages and resistances that are accessible.

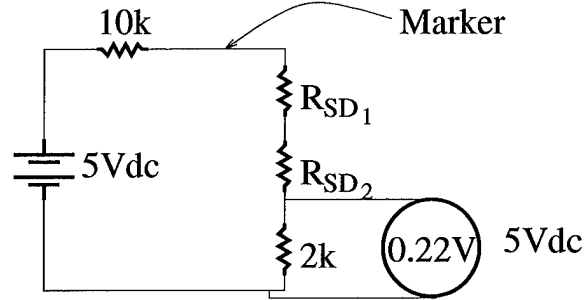


Figure 3.4: Circuit of source impedance measurement

Ohm's Law:

$$V(\text{voltage}) = i(\text{current}) * R(\text{resistance}) \quad (3.1)$$

can be rearranged to read

$$i = V/R \quad (3.2)$$

Using the sampled and measured output value of the brain chip, 0.22 V , and the $2\text{ k}\Omega$ shunting resistor,

$$i = \frac{0.22 V}{2 k\Omega} = 0.11 mA \quad (3.3)$$

Now, re-substituting into equation 3.2 for the entire circuit:

$$0.11 mA = \frac{5 V}{10 k\Omega + R_{SD_1} + R_{SD_2} + 2 k\Omega} \quad (3.4)$$

Therefore:

$$R_{SD_1} + R_{SD_2} \approx \underline{\underline{33 k\Omega}} \quad (3.5)$$

This value is reasonably low, allowing the use of a small shunting resistor, without voltage dividing the signal to immeasurable levels.

Leakage noise was measured via the circuit shown in figure 3.3. Noise was apparent and cycled every 256 samples (corresponding to the neighboring sensor pad). However, placing a $2 k\Omega$ resistor between the signal and ground, to simulate resistance on the cortical surface, removed all signs of this noise signal. Additionally, the source voltage for the noise measurements was approximately 1,000 times larger than the largest expected on the brain. This source was most likely capacitively coupling with the neighboring pads. Therefore, we do not expect to effect the brain's electrical activity.

The next test made certain that a row sync was output from the chip every 16th clock cycle. The oscilloscope showed this signal was pronounced and as expected.

The final test placed a signal on the chip which was systematically reduced to simulate the frequency (5–40 Hz) and magnitude ($10\text{--}200 \mu V_{pp}$) expected on the cortical surface (V_{test} from figure 3.3). This initial series only tested down to $370 \mu V_{pp}$, at 150 Hz. At this point, very high frequency noise becomes apparent. There is, additionally, a standing noise wave riding on the signal ($55 mV_{pp}$), associated with clock ticks (see figure 3.7, page 22, for the nearly identical, but much smaller noise signal of the differential chip.). This noise is substantially reduced from a higher voltage by changing the rise time on the input clock to approximately $5 \mu\text{seconds}$. Additionally, bandpassing the amplifier at $1 k - 30 k Hz$ allows amplification with a gain of 500 without saturating the amplifier. The standing wave is not a problem for sampling because sampling is done at regular intervals, however, the marker voltage must be

reduced to the same amplitude as the noise to avoid saturation. At this point, the oscilloscope is unable to trigger on the marker, and further tests become impossible.

Testing of the reference chip was halted to begin tests on the differential chip, due to the inability to sync the oscilloscope. The differential chip allowed for common mode noise rejection, which has the effect of reducing the standing wave, allowing higher amplification.

Additional noise reduction methods used to get this far are: placing $2\text{ k}\Omega$ shunting resistors from both output and row sync to ground, to draw current; reduction of V_{dd} to 3.1 V .

3.4 Differential Chip

The differential chip, figure 3.5, gains its name from the dual output channels to be used for differential amplification.

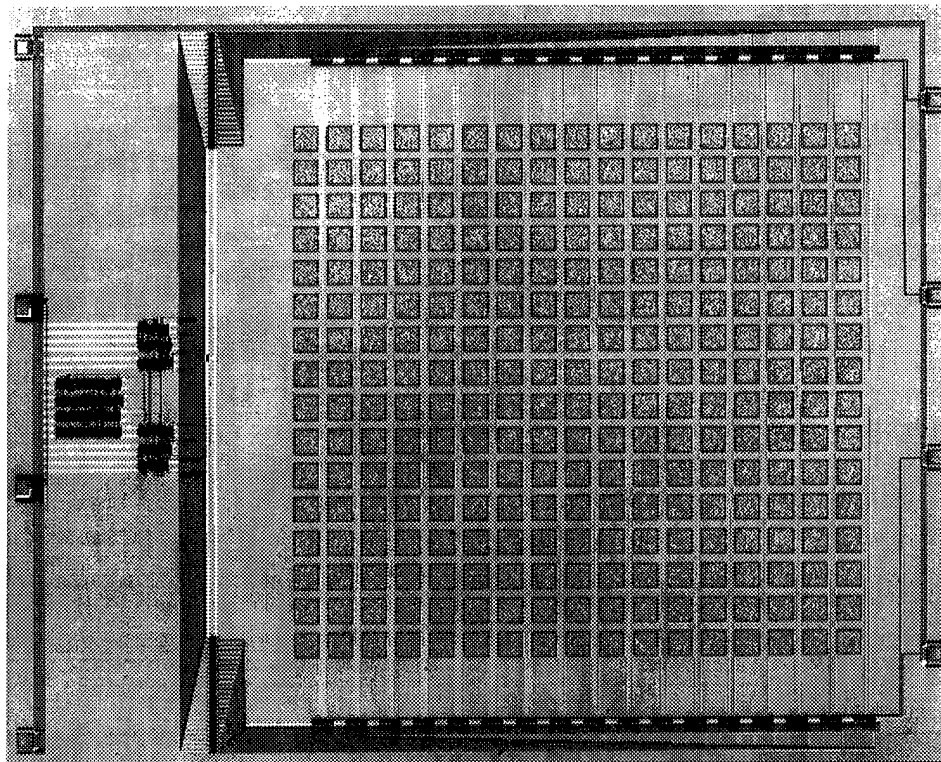


Figure 3.5: Photograph of Differential Chip

3.4.1 Design.

The differential chip was designed with the same requirements as the referenced chip, as well as requirements to improve the signal to noise ratio (Table 3.2). The differential chip

accomplishes this in two ways: differential measurement and dividing the array into two sub-arrays.

Table 3.2: Requirements for Differential Chip [19]

Requirement	Reason	Implemented
Small size	Approximately match the size of individual cortical columns	dime sized
Bidirectional current flow	Allow both stimulation and recording of the cortex	Yes
Small number of I/O connections	Difficulty in making connections from inside the cranium to external circuitry	7
Number of I/O connections not dependent on the number of electrodes	Allows the number of electrodes to be increased without increasing the number of connections	Multiplexing
Capability to individually address the electrodes	Allows stimulation and recording to individual locations of the cortex	Yes
Reduced Noise	Allow amplification of the signal to make precision at least $20\mu V$	Yes

The differential chip consists of two 8×17 sub-arrays, as shown in figure 3.6. In this design two neighboring electrodes, row-wise paired, are connected to two separate output lines, simultaneously. These two lines are then compared using a differential amplifier to remove common mode, or identical, noise. This greatly improves the signal to noise ratio because any noise that one electrode (or it's path to the amplifier) picks up, the identical noise should be picked up by the second electrode. Subtracting one from the other removes this noise and leaves any unique portion of the signal unaffected.

Dividing the array into two sub-arrays improves signal to noise ratio by allowing the clock to run at $1/2$ the frequency required for the reference chip. Because each sub-array has its own output lines, and both sub-arrays are controlled by the same clock, the differential chip outputs two samples to every one sample from the reference chip. Running the clock slower, allows a greater time span to sample the multiplexed output for each chip sample. The data collection section (section 4.4, page 29) describes how averaging multiple samples improves signal to noise ratio.

The differential chip provides a reset instead of a row sync, as provided by the reference chip. The reset allows the tester to synchronize the scanning of the array. The row sync did not allow synchronization of the whole array, it only allowed synchronization to the row

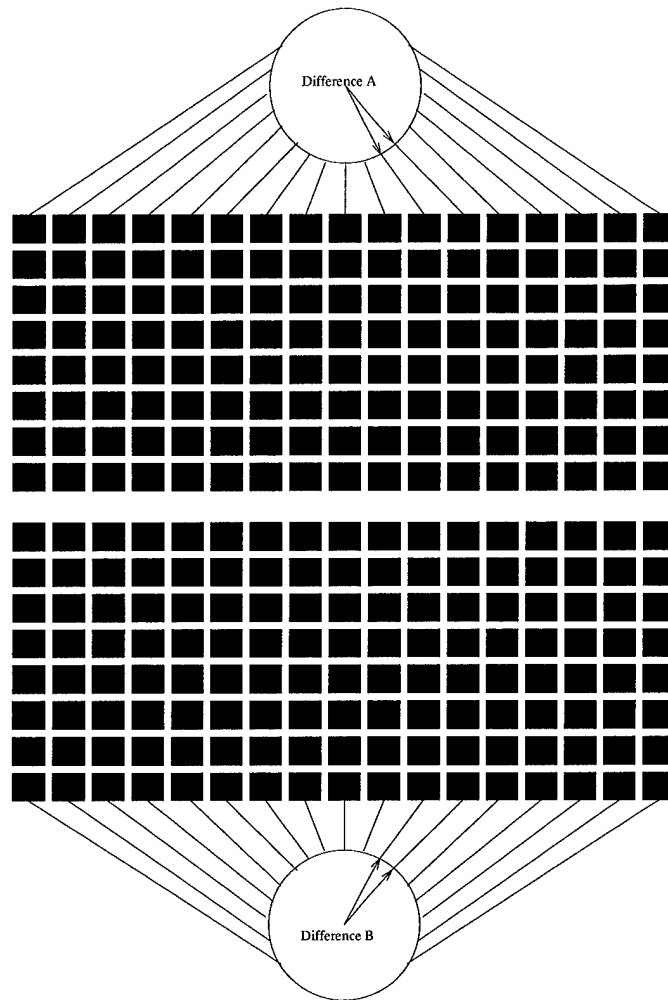


Figure 3.6: Stylized Version of the Differential Chip Design

scans. The row sync left the tester to wonder which pad was being connected to the output line at any one time. This is not the case with the reset.

3.4.2 Testing.

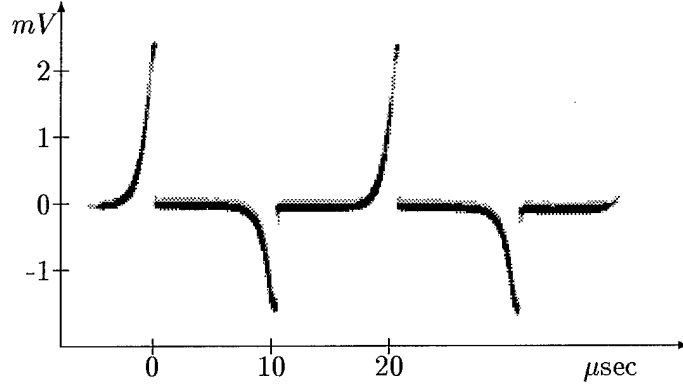


Figure 3.7: Oscilloscope Traces of Output Signal from Differential Chip (Bandpass Filter: $300\text{ Hz} - 10\text{ kHz}$)

The differential chip was tested in the exact same manner as the reference chip, to the point that the reference chip testing was halted due to noise. The differential chip showed a substantial reduction in the standing noise signal, caused by the clock. This allowed amplification with a gain of 2000, compared to 500 for the reference chip. An additional factor in the ability to test with lower input values on the differential chip, is the availability of the reset. The reset allowed the oscilloscope to be triggered without a marker voltage.

Two resistors ($10\text{ k}\Omega$ and $50\text{ }\Omega$) were placed in series with the input signal to perform a voltage division of 200. The divided signal was used as V_{test} . V_{test} was lowered to $20\text{ }\mu\text{V}_{pp}$, and $15\text{ }\mu\text{V}_{pp}$ was measured at the output. This implies a gain on the brain chip of 0.75, however, this is not consistent with readings at higher voltages that imply a gain of 0.28. The gain of 0.28 is what is considered correct, because at $20\text{ }\mu\text{V}_{pp}$ the signal to noise ratio is approximately 1 ($V_{noise} \approx 20\text{ }\mu\text{V}_{pp}$), and precise readings from an oscilloscope become improbable. The amplifier settings used were: gain = 2000 and bandpass was $300\text{ Hz} - 30\text{ kHz}$.

The high frequency nature of the noise found at $20\text{ }\mu\text{V}_{pp}$, figure 3.8 allows oversampling and averaging to improve the signal to noise ratio, and increase the precision. The signal is oversampled by a factor of 16. Because averaging increases the signal by N^2 and the noise by \sqrt{N} , the precision gain is expected to be 64. The estimated precision, where signal to

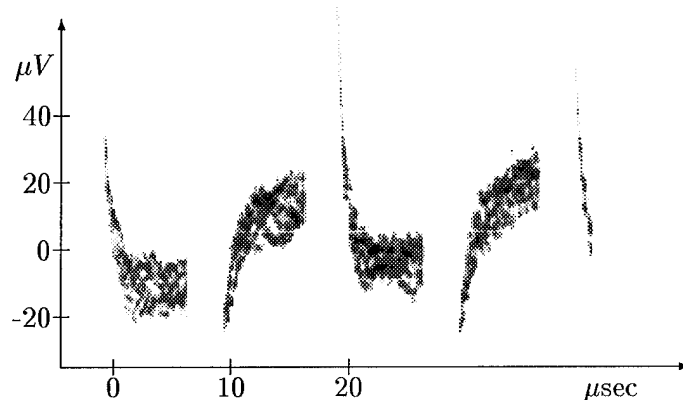


Figure 3.8: Oscilloscope Traces of Output Signal from Differential Chip Containing Approximately $20 \mu V_{pp}$ of High Frequency Noise

noise is expected to be 1 after averaging, is $0.3 \mu V_{pp}$. This will allow measurement of voltage differences over the gambit of levels recorded by other researchers.

During the experiment, all voltages measured must be scaled by the chip gain, to get accurate estimations of the voltage. However, it is the relative activity, and not the exact voltages that is of interest.

3.5 Passivation

Passivation of the brain chips is required to protect the chips in the semiconductor-hostile environment of the brain [19]. The brain is bathed in cerebral spinal fluid (CSF), consisting primarily of sodium ions, Na^+ , and potassium ions, K^+ . There are two steps in passivation: electrode protection and chip encapsulation.

3.5.1 Electrode Protection.

Protecting the metal pads from the CSF requires the use of a conducting material that does not react in this environment. Because MOSIS only provides aluminum metalization, the AFIT brain chips must be plated with such a non-reactive metal. Work has been performed at AFIT with gold and iridium [19]. For this thesis, chips were coated with either gold or iridium. The full process for preparing the electrodes to be coated with metal can be found in Appendix C.

The processes of both gold and iridium metalization are identical, except for power settings and timing information specified in Appendix C. Both metals require a layer of titanium

on top of the aluminum pads to ensure a good electrical connection through the aluminum oxide layer that always builds up on exposed aluminum. Gold is commonly used for sensing devices, however, iridium carries higher current densities. This makes iridium preferable for stimulation applications. An additional consideration is that the iridium was easier to process.

Additionally, an ultrasound cleaner was used to clear the excess gold. The ultrasound cleaner worked extremely well, and without apparent damage to the surface, as with the cotton swab method. However, during later processing, all of the sensor pads fell off. The ultrasound works because the metal vibrates differently than the silicon, loosening the excess metal, as well as the aluminum pads.

The iridium coating lifted off without excessive use of force, and appears to be the better coating.

3.5.2 Encapsulation.

The metallized chips must be protected from the brain fluid on all areas not metallized. DuPont Pyraline polyimide is a relatively easy substance to use, and meets the requirement of passivation [19]. The full process for polyimide coating the chips is in Appendix C.

The polyimide coating process, while not complex, requires some practice. It is more artistic than exacting. Etching the polyimide can be painstakingly slow, however, over-etching can occur suddenly. Any over-etched chips can be cleaned and reused.

3.6 Final Packaging

The passivated chips must be packaged for implantation and interfaced with the laboratory measurement equipment. To meet these ends, the chip is glued to a header, "...a microwave device package manufactured by the Airpax corporation" [19]. Wires are bonded from the input and output pads on the chip, and the entire package is coated with polyimide, excepting the exposed electrode array. All wire connections are made to the pins extending from the back of the header. The wire connections were protected and strengthened with rubber cement.

3.7 Conclusions and Recommendations

The AFIT differential chip is a superior brain chip to the reference chip. The differential chip has proven itself as an effective measuring device capable of measuring differential voltages of $20\ \mu V$ for visual reading from an oscilloscope, and has a reset that is extremely useful for test purposes.

The high frequency nature of the noise found at $20\ \mu V$, allows oversampling and averaging to improve the signal to noise ratio, and increase the precision. The estimated precision, where signal to noise is expected to be 1 after averaging, is $0.3\ \mu V$.

Two differential chips were successfully metallized with gold and passivated. These chips were wire bound and fully prepared for implantation.

4. Methodology

4.1 Introduction

Achieving thesis goals 2–4, page 3, required substantial preparation, test execution, and data acquisition and analysis. This section explains the approach taken.

4.2 Implantation and Testing

The actual implantation effort was planned and reported in the attached protocol, Appendix B.

4.2.1 Test Instrumentation.

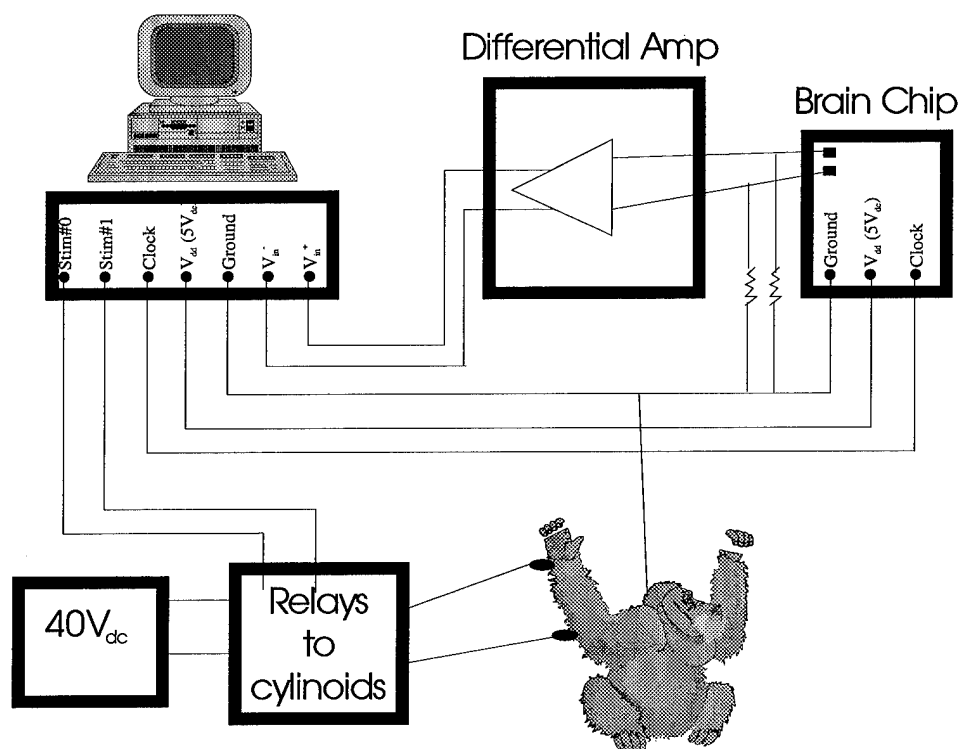


Figure 4.1: Test Equipment Set Up

Five pieces of equipment constitute the test suite: AFIT differential brain chip, Harvard Research differential amplifier, National Instruments AT-MIO-16E-2 data acquisition (DAQ) board (PC insert), 2 relays, 40 V_{dc} power supply, and 2 cylinoids. The National Instruments board was installed in a 486 PC-clone equipped with 16 Mbytes of random access memory

and was augmented with shielded cabling and a National Instruments SCB-68 68-pin shielded connector block to reduce noise.

The DAQ board sends 10 mseconds width pulses, that activate the relays (either #1 or #2), closing a circuit with the $40 V_{dc}$ power supply and cylinoids #1 or #2, which provides a sharp tap for tactile stimulation. The DAQ board simultaneously initiates data acquisition. Voltage differences on the cortex are measured between neighboring sensor pads on the AFIT brain chip. The output of neighboring pads are referenced to ground and amplified differentially by the Harvard Research differential amplifier (band width: 300–30 kHz; gain: 2000). The amplified signal is fed single-ended to the DAQ board, where it is sampled.

Power, ground, and clock for the brain chip are provided by the DAQ board. All signals are directly tied to the DAQ board ground except for the output of the Harvard Research differential amplifier. For this reason, the DAQ board is programmed to measure the difference between the amplifier output and the amplifier's reference, without reference to the DAQ's ground. This measurement method provides common mode rejection for any noise picked up between the amplifier and the DAQ board.

To insure that the input to the differential amplifier will not be overloaded by a static charge on the test subject, the subject must be grounded. This is accomplished with an electrode placed behind the ear of the test subject. Grounding from locations farther from the brain increases the chance of introducing noise from the cardio-pulmonary system.

4.3 Development of Test Scenarios

There are two test scenarios developed and reported herein: averaged evoked response (AER), and apparent motion. The AER test scenario was developed to show that the AFIT array could take usable electro-encephalogram measures from a living animal's cerebral cortex. The apparent motion test scenario was developed to use the AFIT array's capability to record cortical activity during what is subjectively an apparent motion illusion for human's, on the cortex of a living animal.

4.3.1 Averaged Evoked Response (AER) Test.

The sensory evoked response is the voltage signal that can be recorded on the cortex after and corresponding to a stimulus. Dr. Libet refers to the averaged evoked response, the algebraic average of multiple identical stimulus-recording data sets, because a single SER

recording has a very low signal to noise ratio [11, 20]. For all experiments herein, the AER is obtained by averaging recorded responses to 50 identical stimulations. The expected results can be seen in figure 4.2, with a somewhat lower SNR because we are using 50 stimulations, versus 256 per Libet [11]. Additional variation can be expected because this thesis reports measurements taken from the cortex of a rhesus monkey, not a human, as in figure 4.2

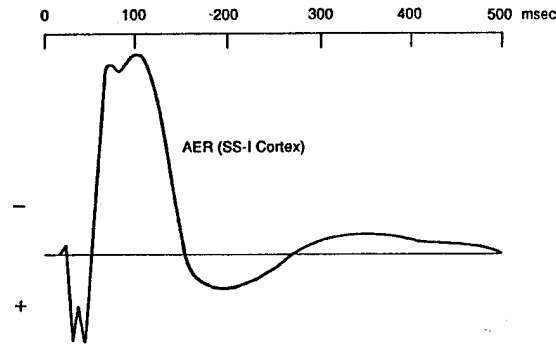


Figure 4.2: Averaged Evoked Response in Human, Using 256 Instances [11]

Because stimulation is performed in an analogous manner to Dr. Libet's, the large peak response is expected at approximately 100 ms after the stimulus.

4.3.2 Apparent Motion Test Setup.

The apparent motion test is based on Geldard and Sherrick's cutaneous rabbit illusion, reported in section 2.2, page 8. To recreate the illusion, where rhythmic tactile stimulations at discrete locations feels like evenly spaced stimulations (hopping rabbit), two identical cutaneous stimulators are used [4]. These are the same stimulators, as used in the AER scenario.

There are three sequences of stimuli required for this scenario, one illusory and two control sequences. The illusory sequence consists of two stimuli of 2 msec duration and 50 msec separation at location 1, followed by 3 stimuli of equal duration and separation, to maintain rhythm, at location 2. The two control sequences consist of identical stimuli and timing, however, one maintains all taps at location 1 and the other maintains them at location 2. The controls will allow post processing to remove any signal information related to position of stimuli and timing of repeated stimuli, leaving only the apparent motion artifacts (assuming that there are any to be recorded).

4.4 Data Collection

Data is collected during all test scenarios in the same manner. The National Instruments DAQ board drives the brain chip with a 20 kHz clock signal, and acquires 16 evenly spaced samples per clock cycle, for a sample rate of 320 kHz. 16 samples are taken per clock cycle so that they can be averaged to increase the measurement system's signal to noise ratio, removing high frequency noise introduced by multiplexing and amplifying the measures brain activity (see figure 4.3). Because averaging increases the signal by N^2 and the noise by \sqrt{N} , the precision gain is expected to be 64. The estimated precision, where signal to noise is expected to be 1 after averaging, is $0.3 \mu V_{pp}$. This should not be confused with the averaging done to improve the signal to noise ratio of the sensory evoked response (noise from within the brain).

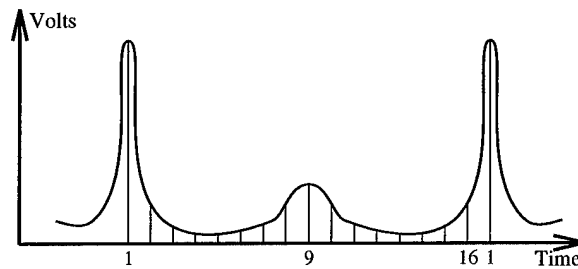


Figure 4.3: Over-sampling the Multiplexed Output

Data is recorded in this fashion for a half a second for each experiment iteration. At the end of this time period the 1/2 second's worth of data is:

1. Averaged in increments of 16, to reduce SNR as stated earlier, and then demultiplexed. This reduces the amount of data samples from 159,744 to 9984 (approximately 1/2 second at 20 ksamples/sec)
2. Demultiplexed into 128 different sensor-related signals, representing 1/2 of the chip. This places the 9984 samples into 128 series each containing 78 data points for the 1/2 second. This meets the Nyquist criteria for sampling frequencies up to 78 Hz.
3. Stored to disk.

Appendix A contains the C-code responsible for initializing the hardware, controlling the experiments, demultiplexing and compiling the results. Additionally, the program allows a sensor to be chosen for display of a running average response.

Experience running this program on a 486 has shown that the minimum memory required is 16 Mbytes. At 8 Mbytes the hard disk is required for virtual memory and the performance plummets.

4.5 Conclusions

Completed preparation for experimentation required successful implementation and testing of the software used to control the National Instruments data acquisition boards; successful design and development of the measurement and amplification circuitry; and successful design and development of the stimulation system.

The central theme of this design is the National Instruments board, which allowed all activity to be synchronized. All portions of this section were successfully implemented and tested. Additionally, the ability to oversample increases the effective precision to $0.3\ \mu V$.

5. Results and Conclusions

5.1 Surgery

Dr. James R. Cooper, AL/OEVM, performed the surgery on an adult rhesus monkey on 25 October, 1995. The monkey had a terminal cancer and was to be euthanized that same day. The monkey was under general anesthesia for the entire experiment (halothane and nitrous oxide), and was euthanized immediately following the experiment. The procedure successfully exposed the gyrus postcentralis (see figure 5.1), where the somatosensory cortex is expected to exist.

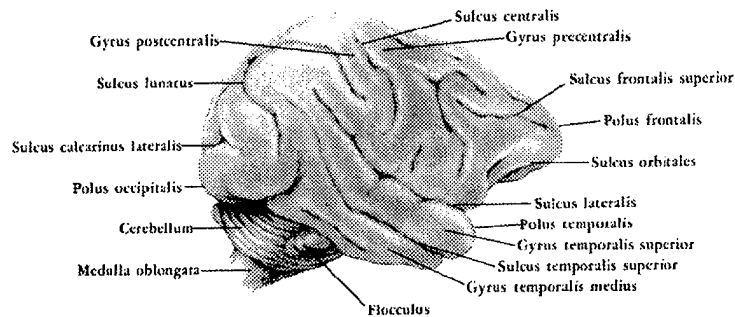


Figure 5.1: Labeled Baboon Brain, Used to Locate the Gyrus Postcentralis [22]

During the experiment, two chips were used and data were recorded for all experiments with each chip. In both cases, bubbles were observed emanating from beneath the chip shortly after contacting the brain. Additionally, a substance that appeared to be polyimide was observed coming from under the chips. After completion of each experiment, damage was observed in the brain tissue immediately under the chip. The damage appeared to be a burn. The monkey's brain was sent for an autopsy, and the subsequent results will shed additional light on the EEG recordings taken.

The most probable cause of the coating problems is that a different polyimide, PI-2722, was unknowingly used, with the same process as for the polyimide used in past work at AFIT. The cure temperature was not high enough to meet recommendations for PI-2722. All instruments and references have been updated in this thesis to avoid this mistake in the future.

5.2 Results

Data were collected corresponding to tests with both chips. All tests were conducted: averaged evoked response (1 test series with each stimulator), apparent motion, apparent motion controls (2 test series using same sequence as apparent motion, but all taps being delivered at the same location). For the first chip, after the first 15 iterations (out of 250), a substantial signal was introduced. This signal, figure 5.2, is evidently caused by the clock. The second chip experienced the same problem after 25 iterations.

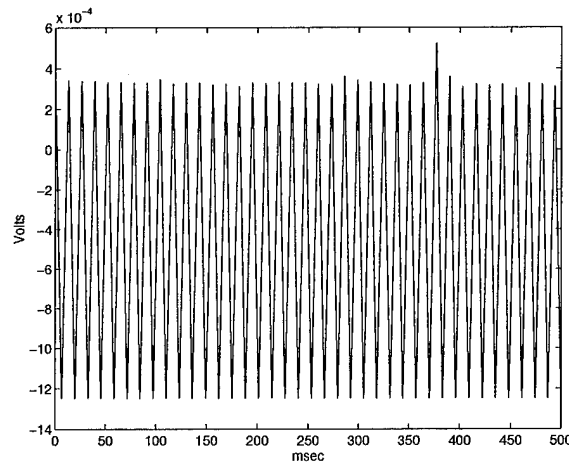


Figure 5.2: Clock Noise Measured with Second Brain Chip—78 samples over 500 msec

After approximately 30 minutes, the clock noise on chip 1, reduced and disappeared. The chip was functional through the entire period, and after the noise died down, the signal in figure 5.10 was recorded.

All plots contained within this report show a time sequence of 78 samples taken in 1/2 second. The vertical scale is in volts. Because of clock noise, none of the apparent motion data is considered valid.

5.2.1 Averaged Evoked Response.

Figure 5.3 shows plots of the EEG signal at one of the sensor locations on the second chip. The top plot shows a single instance (iteration) of EEG data, while, the bottom shows the average of 15 iterations at the same sensor location as in the top plot.

Figure 5.4 shows the averaged evoked response observed in data from the second chip. The plot was obtained by averaging first across iterations 1 thru 25 of the AER experiments,

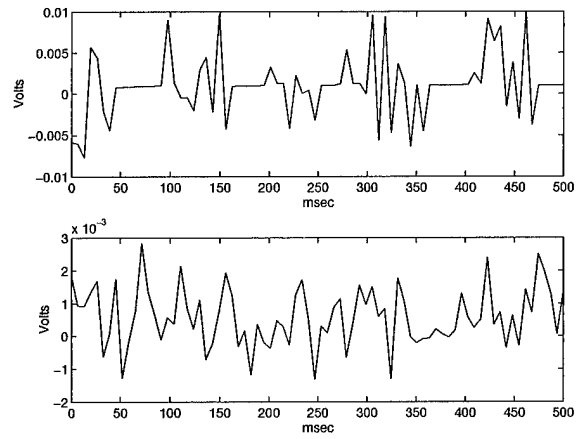


Figure 5.3: Single Sensor Measurement: Sensor 40, with single iteration 15 on top and average of iterations 1 to 15 on bottom—78 samples over 500 msec

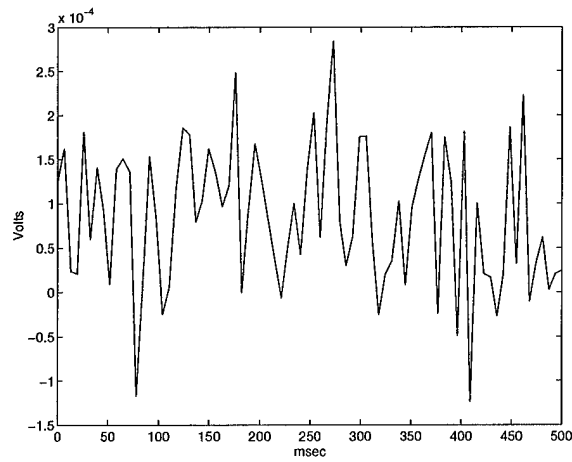


Figure 5.4: Recorded Averaged Evoked Response: First Chip, Average of All Sensors Over 15 Iterations—78 samples over 500 msec

and then averaging across all 128 sensor readings. As is evident, the signal is less pronounced than that in figure 5.5, coming from only 15 samples.

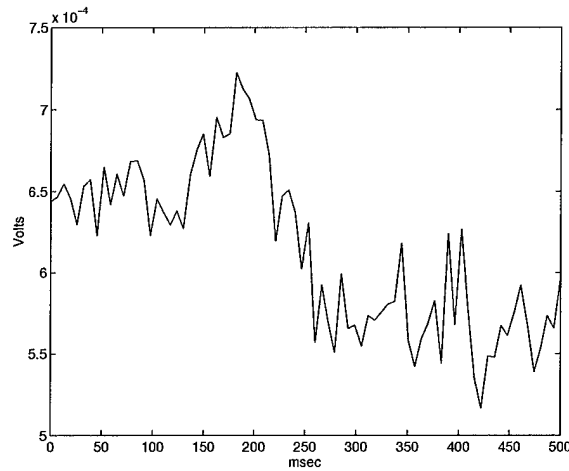


Figure 5.5: Recorded Averaged Evoked Response: Average of All Sensors Over 25 Iterations with Second Chip—78 samples over 500 msec

Figure 5.5 shows the averaged evoked response observed in data from the second chip. The plot was obtained by averaging first across iterations 1 thru 25 of the AER experiments, and then averaging across all 128 sensor readings. The signal to noise ratio is poor, due predominantly to the small data set used. The plot shows a wave with an amplitude swing of approximately $150 \mu V_{pp}$, and a period for the half cycle shown of $1/2$ second. To compare this signal with figure 4.2, page 28, the main peak occurs approximately 190 msec after the stimulus instead of 100 msec. However, they are similar in that a dip immediately precedes the peak in both cases.

5.2.2 Phase Reversal.

To further characterize the performance of the array, the average of all sensors in the top $1/2$ of the chip is compared to the bottom $1/2$, using the same data set used for figure 5.5. The resulting plot, figure 5.6, shows substantial phase reversal. The most obvious conclusion to be drawn is that the source of the signal lies roughly along the center line between the top and bottom halves of the chip.

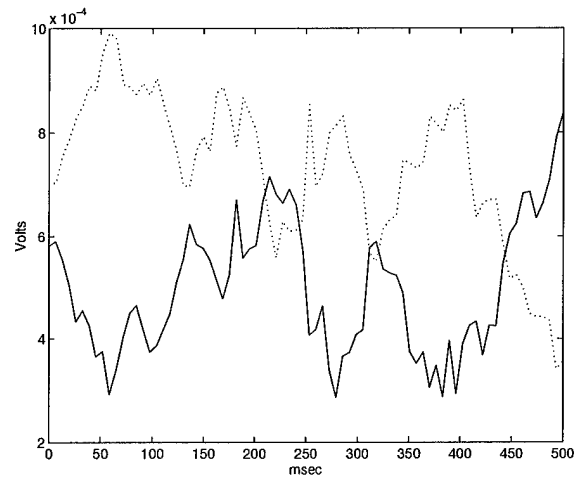


Figure 5.6: Recorded Averaged Evoked Response: Average of All Sensors Over 25 Iterations with Second Chip (Top vs. Bottom)—78 samples over 500 msec

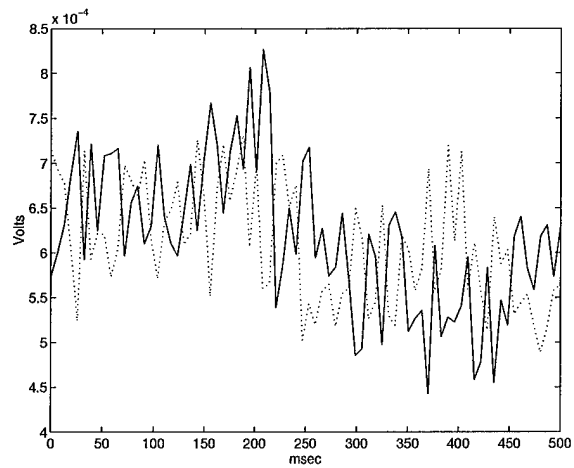


Figure 5.7: Recorded Averaged Evoked Response: Average of All Sensors Over 25 Iterations with Second Chip (Right vs. Left)—78 samples over 500 msec

Figure 5.7 shows another view of the same data. However, in this case, the array is divided into left and right halves. Once again, there is substantial phase reversal, indicating a signal source roughly centered on the chip.

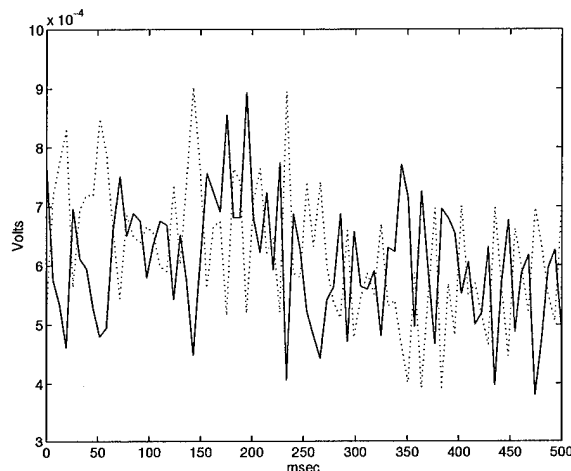


Figure 5.8: Recorded Averaged Evoked Response: Average of All Sensors Over 25 Iterations with Second Chip (Every Other)—78 samples over 500 msec

Figure 5.8 shows yet another view of the same data set. This view takes all of the even numbered sensor locations and plots them against the odd numbered sensors, as seen in figure 5.9. The substantial phase reversal correlates with the concept of measuring at the cortical column level. That is, if signals are being produced at centers (cortical columns) spaced approximately the same distance as the electrodes we would expect phase reversal at the individual electrode level.

5.2.3 Post Noise Saturation Period.

Figure 5.10 shows data recorded with the first chip, after the period of noise saturation. What appears to be an evoked response is clearly visible ($\approx 100 \mu V_{pp}$), with a substantially improved signal to noise ratio. This signal cannot be an artifact of other activity, because it is synchronized with the presentation of a stimulus. The stimulus was not presented at an exact interval because of the Microsoft Windows interrupt driven environment.

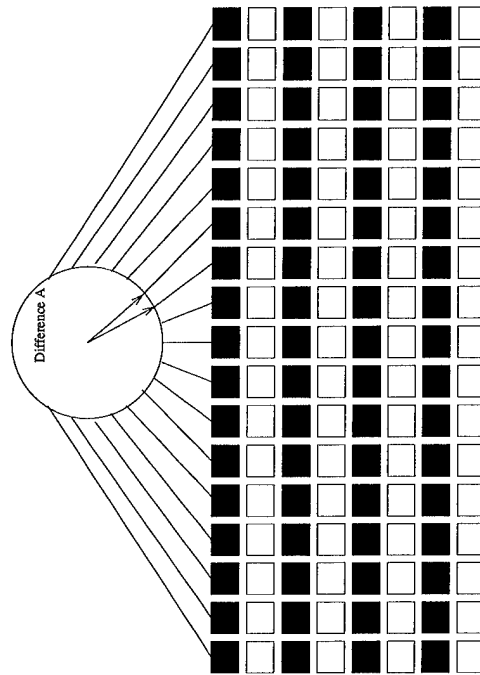


Figure 5.9: Every Other Sensor Selection

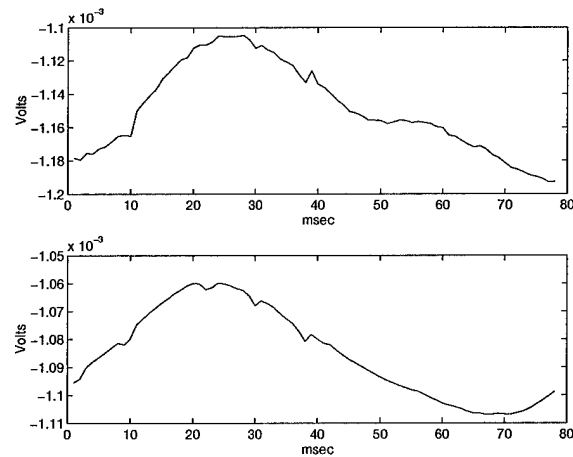


Figure 5.10: Recorded Signals After Noise Saturation—78 samples over 500 msec

5.3 Conclusion

The differential brain chip has proven its ability to record data from the cortex. While there were problems that kept the chip from recording apparent motion signals, the chip continued to work and allowed recording of data after the coating failed. It is apparent that the spacing of the sensor pads is appropriate, at least for rhesus monkeys, to measure at the cortical column scale.

The entire test setup worked, excepting the failure of the chip passivation, and allowed collection of substantial data. A pronounced AEG has been reported, and additional information lies within the recorded data, as yet, undiscovered. Additional work that can be accomplished with the data involves toposcopic views of the activity in the cortical area that was directly under the chip and the relation of the extremely low noise signal discovered after damage was done to the cortex to the actual autopsy findings.

Work must be done to improve the passivation so that the chip does not harm the brain, as was the case in this experiment.

Appendix A: C-Code for Test Scenario Control

```
// **** Brain Chip Data Acquisition Program **** //

#include <windows.h>
#include <conio.h>
#include <stdio.h>
#include <math.h>
#include "wdaq_bc.h"
#include "nidaqcns.h"

#define num_channels 16 // Sample each mux cycle num_channels times
#define gain 1 // Gain of input amplifier
#define num_pads 128 // Number of sensors in mux signal
#define num_mux_samps 9984 // Approx .5 sec. at 20kHz
#define num_dmux_samps 78 // What's left after downsampling and demux
#define num_samples 159744 // num_mux_samps*num_channels
#define samp_int 62 // floor(1/(mux_freq*#channels*int_clk_res))
#define out_rate 100 // Rate of output
int experiment; // Counter for which of 5 experiments to run
int iteration; // How many times an experiment has run
int Error; // Records error codes
int i,j,k; // Generic counters
long l; // Long counter to use with huge arrays
int sync; // Used to align the demuxed signals
double sync_value; // Used to align the demuxed signals
double max; // Used to display plot
HANDLE hsampbuffer=0; // Handle for the sample buffer
int huge *ipsampbuffer; // Big pointer to sample buffer (for locked)
HANDLE hvoltbuffer=0; // Handle for the pre-demuxed voltage levels
double huge *ipvoltbuffer; // Big pointer (for locked)
HANDLE hset1out=0; // Handle for set 1 out buffer
int huge *ipset1out; // Big pointer to above (for locked)
HANDLE hset2out1=0; // Handle for set 2 out1 buffer
int huge *ipset2out1; // Big pointer to above (for locked)
HANDLE hset2out2=0; // Handle for set 2 out2 buffer
```

```

int huge *ipset2out2; // Big pointer to above (for locked)
float huge data[128][78]; // Holder for data to put to file
float cum_data[78]; // Cumulative data to plot
double accumd; // Used to average voltages
float accum; // Used for other accumulations
int stopped; // Whether or not the DAQ stopped
unsigned long samples; // # samples actually collected
int out_ch0=0; // Output on DAC0
int out_ch1=1; // Output on DAC1
double set1out[3]={-.5,5,-.5}; // Experiments 1 & 2
double set2out1[10]= // Experiments 3, 4 & 5, 1st sequence
{-.5,5,-.5,-.5,-.5,-.5,5,-.5,-.5,-.5};
double set2out2[13]= // Experiments 3, 4 & 5, 2nd sequence
{-.5,5,-.5,-.5,-.5,-.5,5,-.5,-.5,-.5,5,-.5,-.5};
int in_chan_vct[num_channels]= // Vector defining the sequence to scan
{0,0,0,0,0,0,0,0,0,0,0,0,0,0,0,0};
int gain_vector[num_channels]= // Vector of associated gain settings
{gain,gain,gain,gain,gain,gain,gain,gain,gain,
gain,gain,gain,gain,gain,gain,gain};
FILE *FID; // File to store data in

// *** Initialize Settings on the NI-DAQ Board *** //
void initialize(void)
{
// *** Initialize Input Portion of the Board *** //
if(Error=AI_Configure(1,0,2,0,0,0)) // AI_0 is single ended,
printf("AI_Configure failed %d",Error); // Nonreferenced and bipolar
if(Error=DAQ_Config(1,1,2)) // Set for external trigger
printf("DAQ_Config failed %d",Error); // and ext. scan-interval
if(Error=Select_Signal(1,ND_IN_SCAN_START,// Scan-interval set to
ND_PFI_9,ND_LOW_TO_HIGH)) // utilize Freq_Out for
printf("Scan-interval not set %d",Error); // synchrony
if(Error=Select_Signal(1,ND_IN_START_TRIGGER,// Use stimulus on
ND_PFI_0,ND_LOW_TO_HIGH)) // ferret as trigger
printf("Trigger not set %d",Error);

```

```

if(Error=Select_Signal(1,ND_FREQ_OUT,// Freq_Out set to 20kHz to
ND_INTERNAL_100_KHZ,5)) // drive brainchip and scan-
printf("Freq_Out not set %d",Error);    // interval

// *** Clear Output Channels to Avoid Spurious Levels *** //
if(Error=AO_VWrite(1,0,-.5)) //Clear output channel 0
printf("Clearing output failed %d",Error);
if(Error=AO_VWrite(1,1,-.5)) //Clear output channel 1
printf("Clearing output failed %d",Error);
}

int main(void)
{
USE_E_Series; // just bring in usable functions

    // *** Set Up Buffers for Data Transfers to and from NI-DAQ Board *** //
hsampbuffer=(HANDLE)GlobalAlloc(GMEM_MOVEABLE,// Allocate an acq.
(DWORD)sizeof(int)*num_samples); // buffer for DMA
ipsampbuffer=(int huge *)GlobalLock(hsampbuffer); // Lock it
hvoltbuffer=(HANDLE)GlobalAlloc(GMEM_MOVEABLE,// Allocate a voltage
(DWORD)sizeof(double)*num_samples); // buffer for conversion
ipvoltbuffer=(double huge *)GlobalLock(hvoltbuffer); // Lock it
hset1out=(HANDLE)GlobalAlloc(GMEM_MOVEABLE,// Allocate an Output
(DWORD)sizeof(int)*3); // buffer
ipset1out=(int huge *)GlobalLock(hset1out); // Lock it
hset2out1=(HANDLE)GlobalAlloc(GMEM_MOVEABLE,// Allocate an Output
(DWORD)sizeof(int)*6); // buffer
ipset2out1=(int huge *)GlobalLock(hset2out1); // Lock it
hset2out2=(HANDLE)GlobalAlloc(GMEM_MOVEABLE,// Allocate an Output
(DWORD)sizeof(int)*9); // buffer
ipset2out2=(int huge *)GlobalLock(hset2out2); // Lock it

// *** Set Up Basic Configuration *** //
initialize();

```

```

// *** Load Test Output Buffers *** //
if(Error=WFM_Scale(1,0,3,1, // Convert voltages to binary
set1out,ipset1out)) // values for output sequence set 1
printf("Output Scaling Failed %d",Error);
if(Error=WFM_Scale(1,0,10,1, // Convert voltages to binary
set2out1,ipset2out1)) // values for output sequence set 1
printf("Output Scaling Failed %d",Error);
if(Error=WFM_Scale(1,0,13,1, // Convert voltages to binary
set2out2,ipset2out2)) // values for output sequence set 1
printf("Output Scaling Failed %d",Error);

// *** Go Through All Five Experiments *** //
for(experiment=0;experiment<5;experiment++)
{
switch(experiment+1)
{
case 1: if(Error=Select_Signal(1, // Use stimulus (pos#0) on
ND_IN_START_TRIGGER, // ferret as trigger
ND_PFI_0,ND_LOW_TO_HIGH))
printf("Trigger not set %d",Error);
FID=fopen("exp1.txt","w"); // Create file to save to
break;
case 2: if(Error=Select_Signal(1, // Use stimulus (pos#1) on
ND_IN_START_TRIGGER, // ferret as trigger
ND_PFI_1,ND_LOW_TO_HIGH))
printf("Trigger not set %d",Error);
fclose(FID); // Close previous file
FID=fopen("exp2.txt","w"); // Create file to save to
break;
case 3: if(Error=Select_Signal(1, // Use stimulus (pos#0) on
ND_IN_START_TRIGGER, // ferret as trigger
ND_PFI_0,ND_LOW_TO_HIGH))
printf("Trigger not set %d",Error);
fclose(FID); // Close previous file
FID=fopen("exp3.txt","w"); // Create file to save to

```

```

break;
case 4: if(Error=Select_Signal(1, // Use stimulus (pos#0) on
ND_IN_START_TRIGGER, // ferret as trigger
ND_PFI_0, ND_LOW_TO_HIGH))
printf("Trigger not set %d", Error);
fclose(FID); // Close previous file
FID=fopen("exp4.txt", "w"); // Create file to save to
break;
case 5: if(Error=Select_Signal(1, // Use stimulus (pos#1) on
ND_IN_START_TRIGGER, // ferret as trigger
ND_PFI_1, ND_LOW_TO_HIGH))
printf("Trigger not set %d", Error);
fclose(FID); // Close previous file
FID=fopen("exp5.txt", "w"); // Create file to save to
break;
    }

// *** Do Each Experiment 50 times *** //
for(iteration=0; iteration<50; iteration++)
{

    // *** Set the Trigger on the Analog Input *** //
    if(Error=SCAN_Setup(1, num_channels, // Init scan vectors:
in_chan_vct, gain_vector)) // scan AI_0 repeated
printf("Scan setup failed %d", Error); // set scan sequence
    if(Error=SCAN_Start(1, ipsampbuffer, // Set scan sequence:
num_samples, -3, samp_int, 0, 0)) // ext. scan sync
printf("Scan setup failed %d", Error); // int. samp timebase

    // *** Stimulate the Test Subject *** //
    switch(experiment+1)
    {
    case 1: if(Error=WFM_Op(1, 1, &out_ch0, // Send Seq 1 on DAC0
ipset1out, 3, 1, out_rate)) // For Experiment 1
printf("Output Scaling Failed %d", Error);

```

```

break;
case 2: if(Error=WFM_Op(1,1,&out_ch1,// Send Seq 1 on DAC1
ipset1out,3,1,out_rate)) // For Experiment 2
printf("Output Scaling Failed %d",Error);
break;
case 3: if(Error=WFM_Op(1,1,&out_ch0,// Send Seq 2 on DAC0
ipset2out1,10,1,out_rate)) // For Experiment 3
printf("Output Scaling Failed %d",Error);
if(Error=WFM_Op(1,1,&out_ch1,// Send Seq 2 on DAC1
ipset2out2,13,1,out_rate)) // For Experiment 3
printf("Output Scaling Failed %d",Error);
break;
case 4: if(Error=WFM_Op(1,1,&out_ch0,// Send Seq 2 on DAC0
ipset2out1,10,1,out_rate)) // For Experiment 4
printf("Output Scaling Failed %d",Error);
if(Error=WFM_Op(1,1,&out_ch0,// Send Seq 2 on DAC0
ipset2out2,13,1,out_rate)) // For Experiment 4
printf("Output Scaling Failed %d",Error);
break;
case 5: if(Error=WFM_Op(1,1,&out_ch1,// Send Seq 2 on DAC1
ipset2out1,10,1,out_rate)) // For Experiment 5
printf("Output Scaling Failed %d",Error);
if(Error=WFM_Op(1,1,&out_ch1,// Send Seq 2 on DAC1
ipset2out2,13,1,out_rate)) // For Experiment 5
printf("Output Scaling Failed %d",Error);
break;
    }

// *** Process the Results *** //
do Error=DAQ_Check(1,&stopped,&samples); // Is it soup yet?
while(!stopped);

if(Error=DAQ_VScale(1,0,gain,1,0,// Convert to voltage
num_samples,ipsampbuffer,ipvoltbuffer))
printf("Conversion Failed %d",Error);

```

```

// *** Demultiplex the Results *** //
l=0;
for(i=0;i<num_dmux_samps;i++) // Separate each time sample
for(j=0;j<num_pads;j++)      // Separate each sensor pad
{
    accumd=0;
    for(k=0;k<num_channels;k++) // Average the oversampled
    { // signal to increase SNR
        accumd+=ipvoltbuffer[l];
        l++;
    }

    data[j][i]=(float)accumd/num_channels;
}

// *** Align the demuxed signals so that pads are in order *** //
sync=0; // Initialize the sync
sync_value=10000; // Initialize the sync value
for(i=0;i<num_pads;i++) // Check each pad's signal
{
    accum=0;
    for(j=0;j<10;j++) // Get change in first 10
    accum+=fabs(data[i][j]-data[i][j+1]); // time samples
    if(accum<=sync_value)
    {
        sync=i;
        sync_value=accum;
    }
}

// *** Write the Results to disk *** //
for(i=0;i<num_dmux_samps;i++) // Go through time
{
    accum=0;
    for(j=sync;j<num_pads;j++) // Go through each sensor pad

```



```

{
fprintf(FID,"%f ",data[j][i]); // Write to disk
accum+=data[j][i]; // Total them up to display
}

for(j=0;j<sync;j++) // Do the rest
{
fprintf(FID,"%f ",data[j][i]); // Write to disk
accum+=data[j][i]; // Total them up to display
}

fprintf(FID,"\n"); // Put each on it's own line
    cum_data[i]+=(accum/num_dmux_samps); // Average all sensors
}

// *** Control the display *** //
if(experiment!=0) // If not first experiment
printf("experiment %d iteration %d \n",// Tell where we are
(experiment+1),(iteration+1));
else // Otherwise
{
// *** Display cumulative results *** //
max=0;
for(i=0;i<num_dmux_samps;i++) // Find greatest and least
{
if(max<fabs(cum_data[i]))max=fabs(cum_data[i]);
}

clrscr(); // Clear the screen
for(i=0;i<num_dmux_samps;i++) // Plot
{
gotoxy(i,(12-(int)(11*(cum_data[i]/max))));
printf("*");
}

}

} // End of Iteration FOR Loop

```

```

} // End of Experiment FOR Loop

// *** Clear Output Channels to Avoid Spurious Levels *** //
if(Error=AO_VWrite(1,0,-.5)) //Clear output channel 0
printf("Clearing output failed %d",Error);
if(Error=AO_VWrite(1,1,-.5)) //Clear output channel 1
printf("Clearing output failed %d",Error);

// *** Free Up Memory *** //
GlobalUnlock(hvoltbuffer); // Unlock volt buffer
    GlobalFree(hvoltbuffer); // Give it back
GlobalUnlock(hsampbuffer); // Unlock sample buffer
GlobalFree(hsampbuffer); // Give it back
GlobalUnlock(hset1out); // Unlock out buffer
GlobalFree(hset1out); // Give it back
GlobalUnlock(hset2out1); // Unlock out buffer
GlobalFree(hset2out1); // Give it back
GlobalUnlock(hset2out2); // Unlock out buffer
GlobalFree(hset2out2); // Give it back
    fclose(FID); // Close last file
return 0;
}

```

ANIMAL USE PROTOCOL COVER SHEET

1. Title: A Multielectrode, Multiplexed Silicon Cortical Electrode

2. Purpose of the Study:

To test *in vivo* the performance of a multielectrode, multiplexed cortical electrode. This 16×16 array (256 total) electrode system is designed to both measure naturally occurring distributed cortical activity and to insert two-dimensional data into the cortex. In the later mode it could serve as a visual prosthesis for blindness caused by lesions distal to the cortical mapping of visual data. The electric field measurements taken from the surface of the brain are called electroencephalogram (EEG) tracings which represent the mean excitatory state of the group of neurons lying directly beneath the measuring electrode. The performance of the multielectrode array will be assessed by the ability of the device to record EEG data.

3. DoD Relevancy:

Animal visual systems have certain capabilities which have direct military application. Primates especially have visual systems with high foveal acuity, color discrimination, and gestalt-based form perception. If such capabilities could be duplicated by machine, they would have immediate direct application in the automatic target acquisition and terminal guidance phases of smart missile systems. Current "smart" weapons still require a human operator to find the target and set up a laser based terminal guidance system. Alternatively, the U.S. Army has developed a series of TV-guided, anti-tank missiles in which a TV picture from the missile is transmitted to a human guidance operator who actually "flies" the missile by remote control.

No reliable automatic target locator or flight guidance system based on visual form has ever been put into operational service even though research on this so called "pattern recognition" problem has been vigorously pursued for about forty years. It is clear that there are some fundamental capabilities immanent in mammalian visual systems that we simply do not understand; if these naturally evolved techniques could be discovered from properly instrumented animal visual systems, it might be possible given the current advanced state of electronic fabrication capabilities, to make a fundamental breakthrough in weapon guidance systems.

4. Type and # of Animals:

Species: Macaca mulatta

Sex: Male

Weight: 12 KG

Age: 12 to 15 years

Total number required: 1

Species: Mustela putorius

Sex: Male

Weight: 1 KG

Age: 12 months

Total number required: 3

5. Disposition of Animals:

The study is designed to allow for the animal to return to the colony following surgical removal of the chip. In the event the health of the animal deteriorates or for some other reason, euthanasia is indicated, the animal will be administered sodium pentobarbital intravenously to effect.

6. Principal Investigator/Organization/Extension:

Steven K. Rogers, AFIT/ENG, 255- 6565, x4284

Matthew Kabrisky, AFIT/ENG, 255-9267.

CORTICAL ELECTRODE ANIMAL PROTOCOL

1. **Title:** A Multielectrode, Multiplexed Silicon Cortical Electrode
2. **Project/Task/Work Unit:**
3. **Principal Investigator:**

Steven K. Rogers, AFIT/ENG
Matthew Kabrisky, AFIT/ENG

4. **Associate or Co-Investigators:** James R. Cooper, AL/OEVM
5. **Scientific Objective:**

To test *in vivo* the performance of a multielectrode, multiplexed cortical electrode. This 16×16 array (256 total) electrode system is designed to both measure naturally occurring distributed cortical activity and to insert two-dimensional data into the cortex. In the later mode it could serve as a visual prosthesis for blindness caused by lesions distal to the cortical mapping of visual data. The electric field measurements taken from the surface of the brain are called electroencephalogram (EEG) tracings which represent the mean excitatory state of the group of neurons lying directly beneath the measuring electrode. The performance of the multielectrode array will be assessed by the ability of the device to record EEG data.

6. **Military Relevance:**

Animal visual systems have certain capabilities which have direct military application. Primates especially have visual systems with high foveal acuity, color discrimination, and gestalt-based form perception. If such capabilities could be duplicated by machine, they would have immediate direct application in the automatic target acquisition and terminal guidance phases of smart missile systems. Current "smart" weapons still require a human operator to find the target and set up a laser based terminal guidance system. Alternatively, the US Army has developed a series of TV-guided anti-tank missiles in which a TV picture from the missile is transmitted to a human guidance operator who actually "flies" the missile by remote control.

No reliable automatic target locator or flight guidance system based on visual form has ever been put into operational service even though research on this so called "pattern recognition" problem has been vigorously pursued for about forty years. It is clear that there are some fundamental capabilities immanent in mammalian visual systems that we simply do not understand; if these naturally evolved techniques could be discovered from properly instrumented animal visual systems, it might be possible given the current advanced state of electronic fabrication capabilities, to make a fundamental breakthrough in weapon guidance systems.

7. **Technical Background:**

The AFIT multielectrode array design was based on several key concepts:

- Information is transmitted in a neuron by the generation of electrical impulses known as action potentials.
- The electric field produced by the activity of neurons can be received by an electrode resting on the surface of the cortical tissue.
- The neurons in the cortex are grouped into cortical columns, which consist of several hundred to several thousand neurons functioning together to perform a given task. These cortical columns are believed to be the smallest functional elements in the cortex.

- There is virtually no transmission of data *across* the cortical sheet. The cortical columns are accessed primarily through input/output axons running through the cerebral alba and between the cortex and the brain stem.
- Analysis of the interconnecting matrix between cortical columns may provide new insight to the function of the brain.

Research similar to that being proposed by AFIT relies on the use of macroelectrodes arranged as arrays of either intracortical probes or surface probes. Intracortical probes are designed to penetrate the cortical surface in order to record the response of (or stimulate) small groups of cortical neurons completely in the interior of the cortical column. Surface electrodes, on the other hand, are used to record or stimulate the *group* of neurons directly beneath the electrode. The electric field measurements taken from the brain by macroelectrodes are called electroencephalogram (EEG) tracings. An EEG represents the mean excitatory state of the group of neurons lying in close proximity to the measuring electrode. Therefore, it is reasonable to expect a surface electrode to record the response of the neurons directly below. Whereas the intracortical probes allow studies primarily in the interior of the cortical sheet.

Properties of the intracortical probe concept emphasize the importance of getting more intimate connection to the interior of the cortical column system. They seem to overlook the inevitable damage which these electrodes cause. But the fact that the columns behave as unitary devices leads us to assume that individual columns can be effectively stimulated from the cortical surface ends of the columns as in fact has been done for decades. Therefore, the AFIT electrode is placed on the cortical surface where it will produce little or no trauma to the cortex beneath it and where it will still have access to the columns for recording and stimulation purposes.

Early research using arrays of surface electrodes relied primarily on the use of bundles of very fine wires placed on the surface of the cortex. In 1966 DeMott reported on the use of a 400 electrode array made up of 400 closely spaced (0.25 mm center-to-center) wires. DeMott's results obtained from a variety of animals, demonstrated substantial differences in the behavior of virtually adjacent cortical areas. This behavior is consistent with the existence of distinct functional cortical columns described by Mountcastle (1957) and Hubel and Wiesel (1962).

In 1968 Brindley published the description of a multielectrode visual prosthesis which he had implanted in the primary visual cortex of a blind human volunteer. This electrode system used 80 separate wires arranged in an approximate 8×10 array; each wire was brought out of the subjects skull and connected to a multi-pin electric connector. Electrical stimulation of any one of the electrodes produced the subjective experience of "seeing" a point of light in a specific location of the subject's visual field. Brindley termed these "phosphenes" and considered them as stimlatable pixels. Thus by stimulating them in appropriate combinations he could transmit crude geometrical images to the visual system of a blind person. Needless-to-say, electrical stimulation of the brain causes no physical discomfort to the subject since there are no pain receptors in the cerebral cortex.

In 1974, Dobelle reported replication of this procedure and produced a demonstration movie showing a blind subject reading Braille letters that had been inserted into his visual cortex by stimulating appropriate sets of electrodes. The subject in Dobelle's experiment

had been blind for 10 years and was able to read Braille at 30 letters a minute using a 64 electrode array for phosphene generation.

Semiconductor technology overcomes many of the problems associated with using wire bundle electrodes. Wire electrodes suffered from poor control over their physical and material characteristics, resulting in a lot of variation in measurements. Also, the number of electrode sites was limited by the amount of wires which could be passed through the scalp. With the current semiconductor technology, multiplexing of the data is easily performed, greatly reducing the number of connections through the scalp. A few of the devices made possible by semiconductor fabrication techniques are discussed in the following paragraphs.

Researchers at the University of Michigan have designed a multichannel multiplexed intracortical probe. This device, which resembles a key, is designed to be inserted into the cortical tissue. The probe is typically 15 μm in thickness with a shank width as narrow as 20 μm . Multiple electrode sites are exposed along the length of the shank. The electrode sites are multiplexed together to allow individual electrodes to be used for recording and or stimulation. By attaching multiple probes in a precisely controlled pattern to an orthogonal platform, a three-dimensional array of electrodes is possible. Such a three-dimensional device can be used to monitor neural activity throughout a volume of cortical tissue. However, use of an intracortical probe does traumatize the tissue. Bleeding was observed during experiments using gerbils. Additionally, probe electrodes were found to have been coated with biological material which may affect the recording capabilities of the electrodes.

Jones, et al. at the University of Utah have also developed a three-dimensional intracortical electrode array. This device consists of a micro machined array of 100 silicon "needles" on a $4.2 \times .2 \times 0.12$ mm thick substrate. The tip of each sharpened needle is coated with platinum and functions as the electrode site. The device is being designed for sensory restoration via intracortical electrical stimulation of a sensory cortex. Experimental implantation of the device has been performed on cats with evidence of some intracortical bleeding due to blood vessel damage being observed. Also, only a few electrodes were able to be accessed with their current technique; a demultiplexer chip to allow access to all electrodes was still in development.

Dagnelie, et al. recorded visually evoked potentials (VEPs) in an alert rhesus monkey using an array of 35 electrodes. The electrodes were organized into five bundles of seven wires each, and were implanted on the striate and peristriate visual cortex. The research was performed as a detailed study of cortical mapping but also demonstrated the usefulness of surface measurements in the study of cortical processing.

Bartlett and Doty investigated the ability of monkeys to detect microstimulation of the striate cortex. In their experiments, an array of twelve electrodes were implanted within the representation of central vision in the visual cortex of a monkey. The animal was then trained to respond to the application of 0.2 ms electrical pulses at 50 Hz to its striate cortex. The purpose of this study was to measure the threshold for the detection of stimulus. The threshold for detection of the stimulus ranged from 50 to 250 μA , depending on the depth of penetration into the cortex. Bartlett and Doty did not test the animal's response to any visual stimulus.

A lot is known about how the brain initially analyzes sensory messages. Yet, how the brain combines sensory messages with past experience for recognition is still not known. Freeman believes that a macroscopic view must be adopted in order to understand perception. His research suggests that perception depends not on the action of individual neurons, but on

the simultaneous, cooperative activity of millions of neurons spread throughout the cortex. Freeman's studies were concentrated on the neurons of the olfactory system. Action potentials from the receptor neurons in the nasal passages propagate to an area of the cortex known as the olfactory bulb. From there, new signals are sent to many other parts of the brain. Note that this is very similar to the way visual signals are received by the primary visual cortex. EEG data was collected simultaneously from 60 to 64 electrodes 0.5 mm apart attached to the surface of the olfactory bulb of trained rabbits.

In Freeman's experiments, a "burst" of oscillations could be seen in each EEG tracing when an animal inhaled a familiar scent. All the tracings from the electrode array were suddenly more regular for a few cycles, until the animal exhaled. Also the tracings often had a higher amplitude ($\sim 100 \mu\text{V}$) and frequency (from 20 to 90 Hz). These bursts are labeled as gamma waves denoting the frequency band of the observed oscillations. Evidence of a collective behavior was shown by the presence of a common waveform, or carrier wave, present in each tracing in the sets of burst recordings. Freeman found that it is not the shape of the carrier wave that identifies an odorant. In fact the wave changed every time the animal inhaled. However, when the average amplitude of each electrode's carrier wave was plotted on a grid representing the olfactory bulb surface, a specific amplitude pattern emerged. As long as the animals training was not changed the same map resulted for a particular odorant, even though the carrier wave was different for each sniff.

Freeman found other parts of the brain may exhibit the same chaotic behavior seen in the olfactory system. In fact, he has documented gamma bursts across large cortical regions involved in the recognition of visual images. His research suggests that familiar visual stimuli are also associated with specific amplitude maps of common carrier waves. Freeman predicts that when viewing a drawing in which foreground and background is ambiguous, such that perception alternates between the two images, the amplitude maps will be found to alternate as well. Similar oscillatory responses were discovered in the cortex of cats and the macaque monkey by Gray and Engel.

It seems likely that interconnection systems between coupled arrays of cortex will be multichannel arrays of axial trunks interconnecting two dimensional arrays of cortical elements. Therefore, the two dimensional AFIT array of electrodes should be the best possible arrangement of detection and stimulation to couple to these systems.

Twelve years have past since the implantation of the first AFIT multielectrode array. This device, which consisted of sixteen multiplexed electrodes arranged in a four-by-four array, was implanted on the visual cortex of a laboratory beagle in 1982. The device functioned for fifteen days before being removed and the subject "Ricky" recovered with no apparent side effects. This experiment validated the concept of using multielectrode arrays for neural research; however, it also identified several improvements that were necessary. The improvements included the need for more electrodes, smaller electrodes to better match cortical columns, better fabrication processes to improve the electrical characteristics, and an improved surgical and implantation procedure. In the years since then, several thesis efforts have been made to improve the device design and to solve the problems encountered with the first implementation.

The current design of the AFIT multielectrode array is described in detail by Rob Reid in his 1993 thesis. This device consists of 256 electrodes laid out in a 16×16 array. A photograph of this device is shown in Figure 1. Each electrode can be enabled or disabled individually. An on-chip counter circuit selects each electrode in sequence as controlled by

an external clock input. The electrodes are $160 \times 160 \mu\text{m}$ with a center-to-center spacing of $250 \mu\text{m}$. This device was tested in a saline environment simulating the environment of the brain, and found to function correctly.

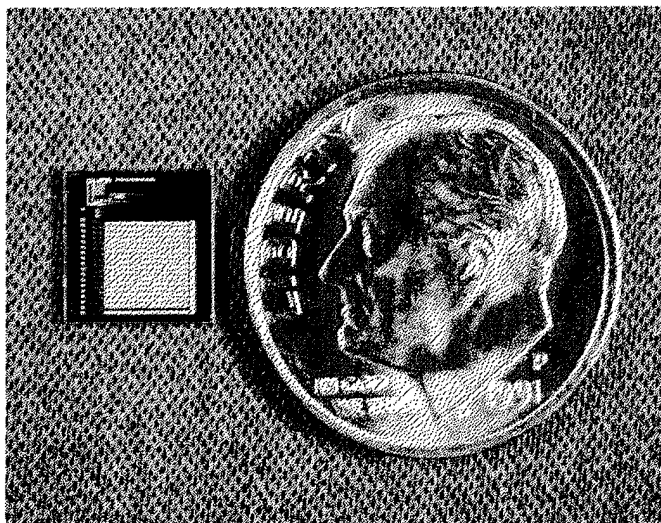


Figure 1. The AFIT multielectrode array.

From the physiological studies, the well known anatomical data, and the research on human volunteers, it is clear that it is possible to insert subjectively perceivable image-like stimuli into mammalian visual systems. Therefore, it is reasonable to assume that if an animal were trained to respond to a specific visual stimuli by, say, pressing a lever to get a food reward, then the insertion of such a visual form directly into its primary visual cortex by electrical stimulus should result in the trained response. Such an experimental result would verify the integrity of the electronic and physiological systems as well as the experimental hypothesis that direct stimulation of animal visual cortex could duplicate the results obtained in human volunteer subjects.

Success at this stage suggests an even more interesting extension of the procedure. While damage to the human primary visual cortex produces only blind spots in the visual field, damage in secondary visual processing areas of the cortex produces categorical visual deficits lumped under the general term: "agnosias". One of these, as an example, prosopagnosia is the complete inability to recognize human faces, even ones own, while retaining otherwise normal visual perception. When a brain so damaged is recovered after death, the only obvious damage is the destruction of a small piece of cerebral cortex in a secondary visual processing area. This leads to postulating a system where visual data are first mapped to primary visual cortex where no significant form analysis (or "perception") occurs since damage there only causes circumscribed blind spots in the visual field. Following this mapping, the visual data are transferred by cortico-cortical tracts in the cerebral alba to secondary visual areas in the cortex where the elegant analysis we call perception actually occurs. Damage to these secondary regions causes catastrophic perceptual disease. It would be of great interest to monitor primary and secondary visual areas simultaneously in an attempt to gather data while the brain is actually performing perception.

Furthermore, it is reasonable to expect that a monkey trained to respond to a certain stimulus such as a light bar at a particular orientation could be used to demonstrate that the

representation of a stimulus is manifested by a particular gamma burst. If the response to the stimulus was recorded and "played back" through a stimulating electrode, the monkey should respond as trained just as if the actual visual stimulus was given. Success of such an experiment would depend on the ability to elicit a cortex-wide burst and also serendipitous placement of the electrodes.

8. Experimental Design:

This experiment will consist of two phases. Phase one will involve the use of ferrets to verify that the AFIT array is capable of recording EEG data from the cortex. Other investigators have found that the ferret is well suited for studies of the visual system (Jackson and Hickey, 1985). Phase two will involve the use of a Rhesus monkey. The array will be used in both species for recording and stimulation. Success of these two phases will be determined by the ability of the device to record EEG and VER data.

a. The anesthetic regimen and surgical approach will be the same in both species. Prior to surgery, the animal will be pre-anesthetized with Ketamine HCL (15 mg/kg) and Atrophine (0.04 mg/kg). Once anesthetized, the head will be shaved and prepared for sterile surgery. Surgical anesthesia will be induced using a 3-5% concentration of Isoflurane in combination with a 80/20 mixture of oxygen and nitrous oxide. The animals heart rate, respiratory rate, and blood pressure will be monitored during the surgical procedure.

The surgical procedure will consist of incising the skin and subcutaneous tissues over the visual cortex. The cranial muscles will then be bluntly dissected exposing the skull. A trephine will be used to create a circular opening in the skull. The device, shown in Figure 2, will be mounted in the circular opening in the skull and coupled to an external connector by a thin cable. The chip and associated mounting media will then be bonded to the skull using a polymallent glass ionomer cement. Three stainless steel bone screws will be tapered into the skull at approximately equal distances around the circumference of the trephine opening for use in anchoring the external connector. Liquid dental acrylic will then be poured over the exposed surface of the skull and the anchoring screws forming a skull cap which will be used to provide support for the external connector.

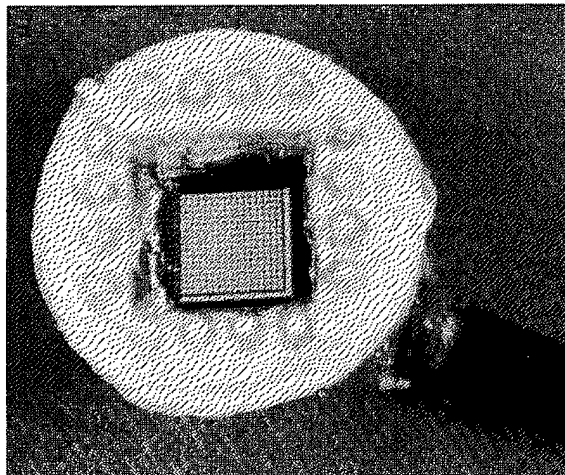


Figure 2. Mounted AFIT Array.

Once the dental acrylic has hardened, the skin and subcutaneous tissues will be apposed to the surface of the skull cap using a pruse string suture pattern. The animal will then be

allowed to recover from anesthesia. An animal caretaker will monitor the animal continuously post surgically until it is able to maintain itself in an upright sitting position.

Seven days following surgery EEG data and Visual Evoked Response (VER) data will be collected from the animal in it's normal awake state. This process will require the animals to be restrained for approximately 10 minutes each day during the recording period. The ferrets will be restrained by simply having a technician hold the animal on their lap. The non-human primate will be restrained by placing the animal in a commercially available restraint chair which has been specifically designed for this species. The monkey will be adapted to the chair during three weeks of training conducted prior to surgery. It is essential that the animals be comfortable and free of distress during the recording period not only for humane reasons but also to assure the validity and reproducibility of the resulting data.

The animal will be monitored as long as the chip is functioning. At the time the chip becomes non-operable it will be removed using identical surgical procedures as were employed during installation. A stainless steel plate will then be placed over the defect in the skull and secured in place using bone screws. The skin incision will be closed using subcutaneous sutures.

b. Statistics: This study will involve only one animal, therefore, no statistical tests will be performed.

9. Literature Review:

A literature search was conducted using Medline, Agricola, and Biological abstracts data bases to assure this study was not a duplication of one already reported in the literature. Based on the results of this search it is determined that this study is unique. Likewise, a DTIC search (search #DKJ35A) conducted on 18 April 1994 revealed no indication that this work has been accomplished previously.

10. Animal Utilization:

Species: Macaca mulatta

Sex: Male

Weight: 12 KG

Age: 12 to 15 years

Total number required: 1

Species: Mustela putorius

Sex: Male

Weight: 1 KG

Age: 12 months

Total number required: 3

a. Three ferrets are requested in phase one of the study in the event that initial testing reveals the chip requires minor modification and/or additional evaluation prior to its implantation into a non-human primate. If the chip appears to be functioning as expected following implantation into the first or second animal, phase one testing will be halted.

b. Use of Alternatives: The use of alternatives such as computer simulations or in vitro techniques were considered. However, the intent of this research is to study the neural electrical activity of the cerebral cortex as it relates to the processing of visual images within the mammalian brain. No in vitro or mechanical system yet developed can approach the level of sophistication required for this study.

c. Rationale: Ferrets were selected for phase-one of the study in an attempt to use the lowest phylogenetic species of animal possible to obtain preliminary data on the operational capabilities of the chip. Primary requirements were that the animal must have a well defined visual cortex and a brain of sufficient size to mount the chip and associated connecting device. Prior research by other authors supports the use of ferrets in visual system research (Jackson and Hickey, 1985; Wen and Shek, 1985).

d. Primate Justification:

(1) There are four primary reasons the non human primate was selected for this study. First, the study requires a species with a brain in which the visual cortex is surgically accessible and of sufficient size to allow placement of a 0.5×0.5 cm chip. Second, later stages of this research will require a species which can be readily trained to respond to visual images originating either through the normal optic pathways or via electrical impulses delivered directly to the visual cortex. Third, use of the non human primate allows more efficient use of data already collected in the highly sophisticated human visual system. Fourth, data obtained from this study will be directly applicable to the human species.

(2) The study is not designed to require euthanasia of the animal.

e. Post Experimental Disposition: Ferrets will be added to an existing ferret colony within the facility. Likewise, the non-human primate will be returned to the primate colony following surgical removal of the chip. In the event the health of the animal deteriorates or for some other reason euthanasia is indicated, sodium pentobarbital will be administered intravenously to the animal in an amount sufficient to elicit a painless death. If euthanasia is performed for the non-human primate due to poor health, it is felt that the body parts would not be useful. On the other hand, if euthanasia is prescribed for reasons other than deteriorating health, an attempt will be made to distribute organs and other body parts to other investigators within the laboratory who may have a requirement for these tissues.

11. Relief of Pain or Distress:

a. This study is classified as category B in the Wright-Patterson AFB "Pain and Distress Classification System." "The research potentially involves minor short-term pain, discomfort or distress which will be treated with appropriate anesthetics/analgesics." The surgical procedures involved in this study would cause pain to the subject animal if not relieved with anesthetic drugs. Human patients who have had similar devices installed within their skulls to record and provide electrical stimulation to their visual cortex have not indicated the procedure was painful.

(1) The animal will be pre anesthetized with Ketamine HCL (15 mg/kg) and atrophine (0.04 mg/kg). Surgical anesthesia will be provided using a 3-5% concentration of Isoflurane superimposed on a 80/20 mixture of oxygen and nitrous oxide. Post-operative analgesia will be provide by administering Buprenorphine (0.01 mg/kg) twice daily by intramuscular injection for 4 days or longer if deemed necessary.

(2) NA

(3) The following data bases were searched in an attempt to determine a less painful or distressful means of conducting this study: Agricola, Biological abstracts and Medline. No less painful or distressful means of conducting the study were found.

(4) Death is not an endpoint in this study. Should the animal become debilitated, loose in excess of 10% of its body weight, refuse to eat or drink, or in some other way indicate that it was in non relievable pain, it will be humanely euthanized.

(5) Dr. John Latandresse DVM/PhD was consulted in the design of this study.

12. Personnel Training:

The surgical procedure will be performed by a veterinarian who has had previous experience in the placement and removal of cortical electrodes and skull caps. All animal manipulations, and post operative care procedures will be performed by personnel certified by the American Association for Laboratory Animal Science (AALAS) at the technologist level.

13. References:

- Bartlett, J.R. and Doty, R.W., "An Exploration of the ability of Macaques to Detect Microstimulation of Striate Cortex," *Acta Neurobiological Experiments*, 40, 713-728, 1980.
- S.L. BeMent, K.D. Wise, D.J. Anderson, K.Najafi, and K.L. Drake, "Solid-State Electrodes for Multichannel Multiplexed Intracortical Neuronal Recording," *IEEE Transactions on Biomedical Engineering*, 33: 230-241 (February 1986).
- G.S. Brindley and W.S. Lewin, "The Sensations Produced by Electrical Stimulation of the Visual Cortex," *Journal of Physiology*, 196: 479-493, 1968.
- G. Dagnelie, H. Spekreijse, and B. VanDijk, "Topography and Homogeneity of Monkey V1 Studied Through Subdurally Recorded Pattern-Evoked Potentials," *Visual Neuroscience*, 3:509-525, 1989.
- D.W. DeMott, "Cortical Micro-toposcopy," *Medical Research Engineering*, 4: 23-29, 1966.
- W.H. Dobelle and M.G. Mladejovsky, "Artificial Vision for the blind: Electrical Stimulation of Visual Cortex Offers Hope for Functional Prosthesis," *Science*, 183: 440- 443 (February 1974).
- W.H. Dobelle, M.G. Mladejovsky, and J.R. Evans, "'Braille' Reading by a Blind Volunteer by Visual cortex Stimulation," *Nature*, 259: 111-112 (January 1976).
- A.K. Engel, et al. "Temporal Coding in the Visual Cortex: New Vista on Integration in the Nervous System," *Trends in Neuroscience*, 15:218-226 (June 1992).
- W.J. Freeman, "The Physiology of Perception," *Scientific American*, 78-85 (February 1991)
- R.W. Hensley and D.C. Denton, "The First Cortical Implant of a Semiconductor Multielectrode Array: Electrode Development and Data Collection", MS thesis, Air Force Institute of Technology, 1982.
- A.C. Hoogerwerf and K.D. Wise, "A Three-Dimensional Neural Recording Array," *Proceedings of the 6th. International Conference on Solid-State Sensors and Actuators*, 120-123 (1991).
- D.H. Hubel and T.W. Weisel, "Receptive Fields and Functional Architecture in Two Non-striate Visual Areas (18 and 19) of the Cat," *Journal of Neurophysiology*, 28:229-289 (1985).
- C.A. Jackson and T.L. Hickey, "Use of Ferrets in Studies of the Visual System," *Laboratory Animal Science*, 35:211-215 (June 1985).
- K.E. Jones, R.J. Huber, K.W. Horch, and R.A. Normann, "A Silicon-Based, Three-Dimensional Neural Interface: Manufacturing Processes for an Intracortical Electrode Array," *IEEE Transactions on Biomedical Engineering*, 38: 758-767 (August 1991).
- M. Kabrisky, et al. "A Multiplexed Multi-electrode Semiconductor Electrode Implant," *IEEE First Annual Conference on Neural networks*, 3:227-242 (June 1987).
- V. B. Mountcastle, "Modality and Topographic Properties of Single Neurons of Cat's Somatic Sensory cortex," *Journal of Neurophysiology*, 20:408-434 (1957).
- J.R. Reid, Jr., "The AFIT Multielectrode Array for Neural Recording and Stimulation: Design, Testing, and Encapsulation," MS thesis, Air Force Institute of Technology, 1993.
- G.Y. Wen, J.A. Sturman, and J.W. Shek, "A Comparative Study of the Tapetum, Retina and Skull of the Ferret, Dog and Cat," *Laboratory Animal Science*, 35:211-215 (June 1985).
- 14. Hazardous Agents:** This study will not employ the use of hazardous agents.
- 15. AFSC Form 3530:** Attached

Appendix C: Post-processing steps

C.1 Standard Clean

1. Mechanically agitate chips in an acetone bath for 30 seconds.
2. Mechanically agitate chips in a methanol or propanol bath for 1 minute.
3. Bake chips at 90° C for 15 minutes.

NOTE: Do not use ultrasound cleaner with chips. It does visually undetectable damage to the chips.

C.2 Metalization Process

1. Clean with standard clean process.
2. Remove from oven and allow to cool.
3. Apply adhesion promoter (HMDS)
 - Puddle HMDS onto the chip. Allow it to spread over the entire chip and coat the edges.
 - Allow to sit for 5 seconds to ensure good coverage of the chip.
 - Spin at 3000 RPM for 45 seconds.
4. Apply positive photo-resist (Shipley AZ1350J)
 - Puddle AZ1350J onto the chip. Allow it to spread over the entire chip and coat the edges.
 - Allow to sit for 5 seconds to ensure good coverage of the chip.
 - Spin at 4000 RPM for 45 seconds.
5. Place chip at the edge of Pyrex container so that only the only one edge of the chip touches the bottom, and two corners touch the side of the container.

NOTE: Chips that are laid flat on the Pyrex dish will become fastened to the bottom, and must be cleaned with the standard clean process before being removed. Otherwise, the chips will break.

6. Pre-bake at 90° C for 20 minutes.
7. Align/Expose for 1.1 minutes.
8. Immerse in chlorobenzene for 10 minutes.
9. Bake at 90° C for 15 minutes.
10. Develop photo-resist.
 - Spin at 500 RPM
 - Spray with AZ351:DIW 1:3 for 45 seconds.
 - Spray with DIW for 30 seconds.
 - Spin dry at 5000 RPM for 45 seconds.
11. Examine pattern. If further develop is necessary, develop for an addition time.
12. Post-Bake at 90° C for 15 minutes.
13. Sputter Ti for 25 minutes with forward power of 200 W (Approx. 300 microns).
14. Sputter Ir for 75 minutes with forward power of 150 W (Approx. 3000 microns).
15. Immerse in acetone bath. Lightly scrub with a cotton swab to ensure all undesired metal is lifted off of the chip.

C.3 Polyimide Application Process

1. Clean chips with the standard clean process.
2. Remove from oven and allow to cool.
3. Apply polyimide (PI-2722):
 - Puddle PI-2722 onto the chip so that it flows over all edges.
 - Allow to sit for 5 seconds to ensure good coverage of the chip.
 - Spin at 3000 RPM for 30 second (Approx. 10 μ m).
4. Soft-bake at 55° C for 90 minutes. - Dries the polyimide without curing.

5. Remove from oven and allow to cool.
6. Align/Expose for 4.5 minutes.
7. Etch the polyimide.
 - Spin at 500 RPM
 - Spray with AZ351:DIW (1:3) for 20 seconds.
 - Overlap spraying with DIW for 7 seconds.
 - Spray with DIW for 20 seconds.
 - Spin dry at 5000 RPM for 30 seconds.
8. Examine to ensure the etch is complete. Etch for additional time if it is required.
9. Final cure at 300° C for 30 minutes. Complete cure of the polyimide.

C.4 Packaging

1. Mount the chip on a header package and wire-bond the connections.
2. Apply a coat of polyimide as follows:
 - Allow polyimide to reach room temperature prior to opening.
 - Using a toothpick, apply polyimide over the wire-bonded connections being careful not to cover any of the electrode array or reference electrode.
3. To avoid expansion and contraction of the polyimide layer which could break wire bonds, the polyimide is cured using gradual changes of temperature as listed in Table C.4.
4. Allow chips to cool in oven.

<i>Temperature (° C)</i>	<i>Time (min.)</i>
70	30
85	30
105	30
130	30
165	360

Table C.1: Cure times for final application of polyimide.

Appendix D: Training Pulse Coupled Neural Networks (PCNN)

The pulse coupled neural network is a detailed model of a biological neuron that exhibits the ability to encode both spatial and temporal signals into a temporal map [6]. The typical PCNN model has three parts: the dendritic tree, linking dendrites and the pulse generator [6, 2]. The dendritic tree is the main pathway for information entering the system, where the feeding input dominates the internal activity. The linking portions of the dendrites allow interaction between neurons, allowing synchronization of firings and modulation of the feeding input. And the pulse generator passes information out of the neuronal model as a synaptic firing. All synapses in this model are viewed as leaky integrators [6, 2]. If a particular neuron's internal activation has risen near its threshold activation level for firing, a linking neuron can fire and push it over the threshold, making it fire synchronously with the linking neuron. Alternatively, the linking neuron could fire and inhibit the subject neuron from firing.

The PCNN, figure D.1, is a basic building block (advanced perceptron) for higher order networks. The linking fields allow an endless number of possible organizations and subsequent logical operations, because linking can inhibit or excite [6]. Additionally, pulse coupling adds a dimension of time to an MLP. Two lower level neurons will have much less effect on an upper level neuron, than if they were synchronized. This is due to the time decay of the internal activation.

D.0.1 Basic Design.

The output, $Y_j(t)$, of a pulse-coupled neural network, using Johnson's design is given by

$$Y_j(t) = \text{step}(U_j(t) - \theta_j(t)) \quad (\text{D.1})$$

[6]. Because the internal activation, $U_j(t)$ increases at a finite rate, while the threshold, $\theta(t)$ increases with an infinite slope at each firing, $Y_j(t)$ is an impulse. When $U_j(t) > \theta_j(t)$ then the neuron fires, raising $\theta_j(t)$ above $U_j(t)$ instantaneously. For discrete time steps it is easier to use

$$Y_j(t) = \begin{cases} 1 & \text{if } U_j(t) \geq \theta_j(t) \\ 0 & \text{otherwise} \end{cases} \quad (\text{D.2})$$

producing a pulse, or firing, output when the total internal activity, $U_j(t)$, rises above the threshold, $\theta_j(t)$ [2].

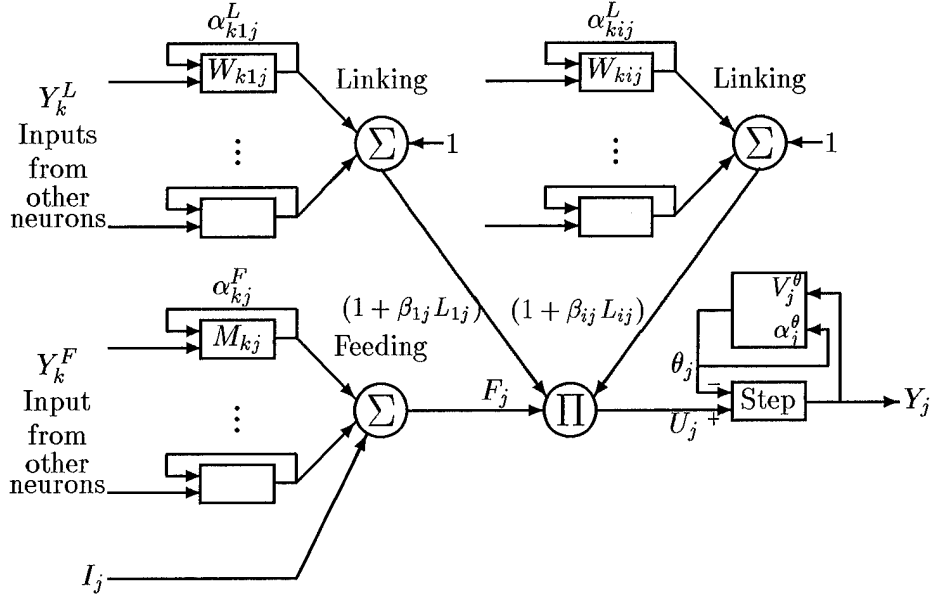


Figure D.1: Pulse Coupled Neural Network [6]

The internal activation, $U_j(t)$, is a function of a feeding input, $F_j(t)$, and any number of linking inputs, $L_{ij}(t)$. The linking inputs are weighted by the linking coefficient, β_{ij} .

$$U_j(t) = F_j(t) \prod_i (1 + \beta_{ij} L_{ij}(t)) \quad (\text{D.3})$$

The feeding input, $F_j(t)$, is a function of an optional analog input, $I_j(t)$, and weighted, summed synaptic inputs from other neurons, $Y_k^F(t)$. Sensory neurons usually do not include inputs from other neurons, while higher level neurons do not typically have an analog input, I_j . Each synapse between the k^{th} feeding neuron and the j^{th} neuron is modeled as a leaky integrator with synaptic weight M_{kj} and decay time constant α_{kj}^F . Therefore,

$$F_j(t) = I_j(t) + \sum_k F_{kj}(t) \quad (\text{D.4})$$

where, using ‘ $*$ ’ as the convolution operator

$$F_{kj}(t) = (M_{kj} e^{-\alpha_{kj}^F t}) * Y_k^F(t) \quad (\text{D.5})$$

[6]. Using a digital filter representation

$$F_{kj}(t) = F_{kj}(t - \Delta t) \cdot e^{-\alpha_{kj}^F \Delta t} + M_{kj} Y_k(t) \quad (\text{D.6})$$

[2].

The i^{th} linking dendrite activity, $L_{ij}(t)$, is a function of weighted, summed synaptic inputs from other neurons, $Y_k(t)$. Each synapse between the k^{th} linking neuron and the i^{th} linking dendritic branch of the j^{th} neuron is modeled as a leaky integrator with synaptic weight W_{kij} and decay time constant α_{kij}^L . Therefore,

$$L_{ij}(t) = \sum_k L_{kij}(t) \quad (D.7)$$

where

$$L_{kij}(t) = (W_{kij}e^{-\alpha_{kij}^L t}) * Y_k^L(t) \quad (D.8)$$

using a digital filter representation

$$L_{kij}(t) = L_{kij}(t - \Delta t) \cdot e^{-\alpha_{kij}^L \Delta t} + W_{kij}Y_k^L(t) \quad (D.9)$$

[6, 2].

The threshold, $\theta_j(t)$, is a function of the output, Y_j , and is also modeled as a leaky integrator with amplitude gain V_j^θ and time constant α_j^θ . θ_{j_0} is added as an offset. $\theta_j(t)$ gets charged every time the neuron fires. This keeps the threshold above the internal activity, so that the neuron isn't in a continuous firing state. The threshold exponentially decays to allow firing to continue after a delay.

$$\theta_j(t) = \theta_{j_0} + (V_j^\theta e^{-\alpha_j^\theta t}) * Y_j(t) \quad (D.10)$$

using a digital filter representation

$$\theta_j(t) = \theta_{j_0} + \theta_j(t - \Delta t) \cdot e^{-\alpha_j^\theta \Delta t} + V_j^\theta Y_j(t) \quad (D.11)$$

[6, 2].

D.0.2 Learning Laws. Most of the literature on PCNNs deals with methods for optical systems which perform image processing, however, the PCNN can be a powerful pattern recognition tool. With standard image processing weights are set by a person to perform a desired task; segmentation or smoothing. To be useful in classification, the PCNN's weights must be adapted based on training samples.

The PCNN can be trained in either a batch or an instantaneous mode. In the batch mode, the PCNN becomes an advanced perceptron or MLP. The instantaneous mode is not quite as common in artificial neural networks, but is very straight forward.

Additionally, a combined learning mode is possible, that can capitalize on the benefits of both previously described modes.

There are two ways to view synchronization for training purposes. First, because synchronized neurons have a stronger effect on the network than unsynchronized, therefore training linking weights in the same batch mode as other weights will capitalize on synchronization. Second, if synchronization is viewed as an end to itself, then linking weights must be updated to cause the desired level of synchronization.

D.0.2.1 Batch Mode: PCNNs as Perceptrons. Both PCNNs and Perceptrons take an input and compute a firing rate based on the input and synaptic weights. The PCNN does perform a more precise encoding of the input than the perceptron because of its temporal firing sequences, but all of the linking could easily be implemented in an MLP by adding feedback loops.

To allow the use of perceptron type learning for a PCNN, a time ‘batch’ must be defined. Therefore, let $\Gamma = n(\Delta t)$ where $n \in \{\text{Naturals}\}$. Now the average firing rate, $\psi_j(b)$ for the period Γ can be computed.

$$\psi_j(b) = \frac{\sum_{w=0}^{\Gamma-1} (Y_j(t_b + w\Delta t))}{\Gamma} \quad (\text{D.12})$$

where b represents the batch process, making t_b the first sample of batch b .

Training the PCNN to reduce the total error requires the following definition of error.

$$E(b) = \frac{1}{2} \sum_{z=1}^J (d_z - \psi_z(b))^2 \quad (\text{D.13})$$

where J is the total number of ‘output’ neurons of interest. These neurons do not have to be output neurons, but they must be neurons for which a desired average firing rate can be asserted. Now, all synaptic and linking weights of the output neurons can be updated in the direction of the negative slope of the error surface, with an arbitrary step size, η .

$$W(b+1) = W(b) - \eta \frac{\partial E(b)}{\partial W} \quad (\text{D.14})$$

where ‘ W ’ represents a generic weight, synaptic or linking.

An algorithmic simplification can be made for multi-layered and/or multi-connected networks, by removing the requirement for a predetermined desired average firing rate. This simplification would be to

1. Apply the error equation to the output neurons based on real desired firing rates
2. Update weights for output neurons (including the linking weights and possibly even the decay time coefficients). Keep a record of the direction and magnitude of each change to synaptic weights. These weight changes will be passed to the input neurons. If the j^{th} neuron increases its synaptic weight for the k^{th} input neuron by 0.1, then the k^{th} input neuron is requested to increase its firing rate by 0.1 (or a scaled amount).
3. For each lower level, or input neuron, total the changes recorded in step 2, associated with the subject neuron. This will give a relative direction and amount of change required in the firing rate ('+' means rate needs to increase '-' means rate needs to decrease). This can be scaled and used as the desired for the lower level.
4. Make sure you did not update weights on a neuron that has already been updated in this batch, to avoid infinite loops.

To update β_{ij} (from equation D.14):

$$\beta_{ij}(b+1) = \beta_{ij}(b) - \eta \frac{\partial E(b)}{\partial \beta_{ij}} \quad (D.15)$$

from equation D.13

$$\frac{\partial E(b)}{\partial \beta_{ij}} = \frac{\partial}{\partial \beta_{ij}} \left[\frac{1}{2} \sum_{z=1}^J (d_z - \psi_z(b))^2 \right] \quad (D.16)$$

$$= \frac{\partial}{\partial \beta_{ij}} \left[\frac{1}{2} \left\{ \dots + (d_j - \psi_j(b))^2 + \dots + (d_J - \psi_J(b))^2 \right\} \right] \quad (D.17)$$

$$= \frac{\partial}{\partial \beta_{ij}} \left[\frac{1}{2} (d_j - \psi_j(b))^2 \right] \quad (D.18)$$

$$= (d_j - \psi_j(b)) (-1) \frac{\partial}{\partial \beta_{ij}} [\psi_j(b)] \quad (D.19)$$

Looking back to equation D.12

$$\frac{\partial \psi_j(b)}{\partial \beta_{ij}} = \frac{\partial}{\partial \beta_{ij}} \left[\frac{\sum_{w=0}^{n-1} (Y_j(t_b + w\Delta t))}{\Gamma} \right] \quad (D.20)$$

$$= \frac{1}{\Gamma} \sum_{w=0}^{n-1} \left\{ \frac{\partial}{\partial \beta_{ij}} [Y_j(t_b + w\Delta t)] \right\} \quad (D.21)$$

From equation D.1, and letting $\tau = t_b + w\Delta t$:

$$\frac{\partial}{\partial \beta_{ij}} Y_j(\tau) = \frac{\partial}{\partial \beta_{ij}} [\text{step}(U_j(\tau) - \theta_j(\tau))] \quad (\text{D.22})$$

At this point, the step function makes direct differentiation impossible. Close inspection, however, shows that the only purpose for continuing the differentiation is to decide whether to increase or decrease the weight in question, or, more specifically, what effect a change in the particular weight will have on the output. The term $(d_j - \psi_j(b))(-1)$, from equation D.19, already determines whether the firing rate needs to be increased or decreased, and by how much.

To continue differentiation, one must capitalize on the nature of the pulse generator, equation D.1. Firing occurs when $U_j(t)$ rises above $\theta_j(t)$. Therefore, increasing $U_j(t)$ will have the effect of increasing the firing rate. The remaining term, $\theta_j(t)$, is solely a function of the output (reference equation D.10), and will therefore not be effected by any change in the weights. Because $Y_j(t)$ relies completely on $U_j(t)$ in a direct fashion, the following substitution will only lose a scaling factor, which can be accounted for in the step size.

$$\frac{\partial}{\partial \beta_{ij}} Y_j(\tau) \rightarrow \frac{\partial}{\partial \beta_{ij}} U_j(\tau) \quad (\text{D.23})$$

$$\frac{\partial}{\partial \beta_{ij}} U_j(\tau) = \frac{\partial}{\partial \beta_{ij}} \left[F_j(\tau) \prod_{z=1}^I (1 + \beta_{zj} L_{zj}(\tau)) \right] \quad (\text{D.24})$$

$$= F_j(\tau) \prod_{z \neq i} (1 + \beta_{zj} L_{zj}(\tau)) \frac{\partial}{\partial \beta_{ij}} [1 + \beta_{ij} L_{ij}(\tau)] \quad (\text{D.25})$$

$$= \frac{U_j(\tau)}{(1 + \beta_{ij} L_{ij}(\tau))} L_{ij}(\tau) \quad (\text{D.26})$$

From equation D.21

$$\frac{\partial \psi_j(b)}{\partial \beta_{ij}} \approx \frac{1}{\Gamma} \sum_{w=0}^{n-1} \left[\frac{U_j}{(1 + \beta_{ij}(b) L_{ij}(\tau))} L_{ij}(\tau) \right] \quad (\text{D.27})$$

Substituting into equations D.15 and D.19

$$\beta_{ij}(b+1) = \beta_{ij}(b) + \frac{\eta}{\Gamma} (d_j - \psi_j(b)) \sum_{w=0}^{n-1} \left[\frac{U_j}{(1 + \beta_{ij}(b) L_{ij}(\tau))} L_{ij}(\tau) \right] \quad (\text{D.28})$$

To update W_{kij} , equation D.25 can be a starting point.

$$\frac{\partial}{\partial W_{kij}} U_j(\tau) = F_j(\tau) \prod_{z \neq i} (1 + \beta_{zj} L_{zj}(\tau)) \frac{\partial}{\partial W_{kij}} [1 + \beta_{ij} L_{ij}(\tau)] \quad (D.29)$$

$$\frac{\partial}{\partial W_{kij}} (1 + \beta_{ij} L_{ij}(\tau)) = \beta_{ij} \frac{\partial}{\partial W_{kij}} L_{ij}(\tau) \quad (D.30)$$

$$= \beta_{ij} \frac{\partial}{\partial W_{kij}} \sum_{z=1}^K L_{zij}(\tau) \quad (D.31)$$

$$= \beta_{ij} \frac{\partial}{\partial W_{kij}} L_{kij}(\tau) \quad (D.32)$$

$$= \beta_{ij} \frac{\partial [L_{kij}(\tau) e^{-\alpha_{kij}^L \Delta \tau} + W_{kij} Y_k^L(\tau)]}{\partial W_{kij}} \quad (D.33)$$

$$= \beta_{ij} Y_k^L(\tau) \quad (D.34)$$

$$W_{ij}(b+1) = W_{ij}(b) + \frac{\eta}{\Gamma} (d_j - \psi_j(b)) \sum_{w=0}^{n-1} \left[\frac{U_j}{(1 + \beta_{ij}(b) L_{ij}(\tau))} Y_k^L(\tau) \right] \quad (D.35)$$

To update M_{kj} , equation D.24

$$\frac{\partial}{\partial M_{kj}} U_j(\tau) = \frac{U_j(\tau)}{F_j(\tau)} \frac{\partial}{\partial M_{kj}} F_j(\tau) \quad (D.36)$$

using equation D.4

$$\frac{\partial}{\partial M_{kj}} F_j(\tau) = \frac{\partial}{\partial M_{kj}} \left[I_j(t) + \sum_{z=1}^K F_{zj}(t) \right] \quad (D.37)$$

$$= \frac{\partial}{\partial M_{kj}} F_{kj}(t) \quad (D.38)$$

$$= \frac{\partial}{\partial M_{kj}} [F_{kij}(\tau) e^{-\alpha_{kij}^F \Delta \tau} + M_{kj} Y_k^F(\tau)] \quad (D.39)$$

$$= Y_k^F(\tau) \quad (D.40)$$

$$M_{kj}(b+1) = M_{kj}(b) + \frac{\eta}{\Gamma} (d_j - \psi_j(b)) \sum_{w=0}^{n-1} \left[\frac{U_j}{F_j(b)} Y_k^F(\tau) \right] \quad (D.41)$$

Using the same derivation as above, a learning rule can be established for all time constants.

D.0.2.2 Instantaneous Mode. Instantaneous mode training can be viewed in a number of ways, all retaining the goal of training the PCNN at each time increment and

based on the information at hand. The particular method used herein considers a synapse as the driving force for weight change.

Competing hypertrophic and atrophic forces, where hypertrophy is caused when a synapse occurs (increasing the weight given to that synapse) and atrophy is a constant exponential decay of the weight, gives a self organizing character to the PCNN. Because, with even a limited amount of linking, this training process may saturate the output of numerous neurons by increasing synaptic and linking weights of symbiotic neurons to unacceptable levels, the learning law must constrain the weights. With this in mind, consider the following learning law.

$$W_t = \left(1 - \frac{1}{\alpha_a}\right) W_{t-\Delta t} + \frac{\alpha_h}{\alpha_a} (1 - W_{t-\Delta t}) Y_{k_t-\Delta t} \quad (\text{D.42})$$

where W_t and $W_{t-\Delta t}$ are the new and previous weights, respectively, to be substituted with M_{kj} , W_{kij} and β_{ij} from equations D.6 and D.9. Also α_a and α_h are the atrophic and hypertrophic factors, respectively, where $\alpha_a > \alpha_h$. This rule keeps all weights between 0 and 1.

Training in this mode requires less memory and CPU time compared to batch mode, but reduces the possible complexity of the neural interaction (whether a linking input excites or inhibits must be predetermined).

D.0.2.3 Combined Mode. This mode uses the fast and simple weight update rule for M_{kj} and W_{kij} , but implements the batch update rule for β_{ij} . This allows the linking weights to inhibit or excite based on the training samples and the desired output, while maintaining the speed of the instantaneous mode.

Bibliography

- [1] DeMott, Donald W. "Cortical Micro-toposcopy," *Medical Research Engineering*, 5(4):23-29 (1966).
- [2] Eckhorn, R., et al. "Feature Linking via Synchronization Among Distributed Assemblies: Simulations of Results from Cat Visual Cortex," *Neural Computation*, 2:293-307 (1990).
- [3] Freeman, Walter J. "The Physiology of Perception," *Scientific American*, 264(2):78-85 (February 1991).
- [4] Geldard, Frank A. and Carl E. Sherrick. "The Cutaneous "Rabbit": A Perceptual Illusion," *Science*, 178(4057):178-179 (October 1972).
- [5] Hubel, D.H. and T.W. Weisel. "Receptive Fields and Functional Architecture in Two Nonstriate Visual Areas (18 and 19) of the Cat," *Journal of Neurophysiology*, 28:229-289 (1965).
- [6] Johnson, John L. "Pulse-Coupled Neural Nets: Translation, Rotation, Scale, Distortion, and Intensity Signal Invariance for Images," *Applied Optics*, 33(26):6239-6253 (10 September 1994).
- [7] Kabrisky, Mathew, et al. "A Multiplexed Multi-Electrode Semiconductor Brain Electrode Implant," *IEEE First Annual International Conference on Neural Networks* (1987). IEEE Catalog #87TH0191-7.
- [8] Kapit, Wynn, et al. *The Physiology Coloring Book*. New York: HarperCollins Publishers, Incorporated, 1987.
- [9] Kinney, Hannah C. and others. "Neuropathological Findings in the Brain of Karen Ann Quinlan," *The New England Journal of Medicine*, 330(21):1469-1475 (May 1994).
- [10] Libet, Dr., Benjamin. "The Neural Time Factor in Conscious and Unconscious Events." *Experimental and Theoretical Studies of Consciousness* 123-146, John Wiley and Sons, 1993.
- [11] Libet, Dr., Benjamin, et al. "Subjective Referral of the Timing For a Conscious Sensory Experience: A Functional Role for the Somatosensory Specific Projection System in Man," *Brain*, 102:193-224 (1979).
- [12] Llinás, R.R. and D. Paré. "Of Dreaming and Wakefulness," *Neuroscience*, 44(3):521-535 (1991).

- [13] Mind and Brain. "Gerald D. Fischbach," *Scientific American*, 267(3) (1992).
- [14] Mishkin, Mortimer and Tim Appenzellar. "The Anatomy of Memory." *The Workings of the Brain: Development, Memory and Perception* edited by Rodolfo R. Llinás, chapter 6, New York: W. H. Freeman and Company, 1990.
- [15] Mumford, Dr., David. "On the Computational Architecture of the Neocortex: The Role of the Thalamo-Cortical Loop," *Biological Cybernetics*, 65:135-145 (1991).
- [16] Mumford, Dr., David. "On the Computational Architecture of the Neocortex: The Role of the Cortico-Cortical Loop," *Biological Cybernetics*, 66:241-251 (1992).
- [17] Nauta, Walle J. H. and Michael Feirtag. "The Organization of the Brain." *The Workings of the Brain: Development, Memory and Perception* edited by Rodolfo R. Llinás, chapter 6, New York: W. H. Freeman and Company, 1990.
- [18] Ojemann, George A. "Effect of Cortical and Subcortical Stimulation on Human Language and Verbal Memory." *Language, Communication, and the Brain* edited by F. Plum, New York: Raven Press, 1988.
- [19] Reid, Jr., James R. *The AFIT Multielectrode Array for Neural Recording and Stimulation: Design, Testing, and Encapsulation*. MS Thesis, Air Force Institution of Technology, 1993.
- [20] Spenik, Adam G. *Experimental Definition for Implantation of the AFIT Cortical Multielectrode Array*. MS Thesis, Air Force Institution of Technology, 1994.
- [21] Stiles, Bryan W. and Joydeep Ghosh. "A Habituation Based Mechanism for Encoding Temporal Information in Artificial Neural Networks." Department of Electrical and Computer Engineering, University of Texas at Austin. Unpublished.
- [22] Swindler, Daris R. and Charles D. Wood. *An Atlas of Primate Gross Anatomy: Baboon, Chimpanzee, and Man*. University of Washington Press, 1973.

Vita

Captain John E. Rosenstengel was born March 27, 1967, in St. Louis, Missouri. In 1989, he graduated from the United States Air Force Academy with a bachelors degree in electrical engineering. Prior to attending AFIT, he was stationed at Los Angeles Air Force Base, with the Air Force Satellite Control Network Program Office. Captain Rosenstengel is married to the former Tracy Ann Lenning of Orange County, California and they have two children, Caprice and Kimberly.

Permanent address: 8949 Cypress Gate Drive
Huber Heights, OH 45424

REPORT DOCUMENTATION PAGE			Form Approved OMB No. 0704-0188	
<small>Public reporting burden for this collection of information is estimated to average 1 hour per response, including the time for reviewing instructions, searching existing data sources, gathering and maintaining the data needed, and completing and reviewing the collection of information. Send comments regarding this burden estimate or any other aspect of this collection of information, including suggestions for reducing this burden, to Washington Headquarters Services, Directorate for Information Operations and Reports, 1215 Jefferson Davis Highway, Suite 1204, Arlington, VA 22202-4302, and to the Office of Management and Budget, Paperwork Reduction Project (0704-0188), Washington, DC 20503.</small>				
1. AGENCY USE ONLY (Leave blank)		2. REPORT DATE December 1995	3. REPORT TYPE AND DATES COVERED Master's Thesis	
4. TITLE AND SUBTITLE Electroencephalography: Subdural Multi-electrode Brain Chip			5. FUNDING NUMBERS	
6. AUTHOR(S) John E. Rosenstengel, Capt, USAF				
7. PERFORMING ORGANIZATION NAME(S) AND ADDRESS(ES) Air Force Institute of Technology, WPAFB OH 45433-6583			8. PERFORMING ORGANIZATION REPORT NUMBER AFIT/GE/ENG/95D-22	
9. SPONSORING / MONITORING AGENCY NAME(S) AND ADDRESS(ES)			10. SPONSORING / MONITORING AGENCY REPORT NUMBER	
11. SUPPLEMENTARY NOTES				
12a. DISTRIBUTION / AVAILABILITY STATEMENT Approved for public release; Distribution Unlimited			12b. DISTRIBUTION CODE	
13. ABSTRACT (Maximum 200 words) In October 1995, a CMOS brain chip consisting of two 8 x 17 multiplexed sub-arrays designed to measure electrical potentials at the cortical column level, was implanted on the somatosensory cortex of a laboratory rhesus monkey. Electroencephalograph (EEG) and averaged evoked response (AEG) data were taken over a period of 40 minutes. The brain chip was replaced with an identical chip, and data were again taken for 40 minutes. In both instances AEG signals of approximately $150 \mu V_{pp}$ were recorded. Additionally, the first implanted chip recorded three phases of data: 1) AEG; 2) large clock noise (during a period where the chip appears to have burned the cortex); 3) AEG-like signals of magnitude, $\approx 100 \mu V_{pp}$, with substantially improved signal to noise ratio. All data were taken while the monkey was under general anesthesia. The monkey was euthanized immediately after the experiments, due to a pre-existing abdominal cancer.				
14. SUBJECT TERMS ELECTROENCEPHALOGRAPHY, BRAIN CHIP, EEG, AVERAGED EVOKED RESPONSE, AEG, SENSORY EVOKED RESPONSE, MULTI-ELECTRODE ARRAY, APPARENT MOTION			15. NUMBER OF PAGES 83	
			16. PRICE CODE	
17. SECURITY CLASSIFICATION OF REPORT UNCLASSIFIED	18. SECURITY CLASSIFICATION OF THIS PAGE UNCLASSIFIED	19. SECURITY CLASSIFICATION OF ABSTRACT UNCLASSIFIED	20. LIMITATION OF ABSTRACT UL	